Cellular and Molecular Life Sciences

ORIGINAL ARTICLE | Article in Press

A nutrient-sensitive CPT1C-ABHD6 axis regulates BMP homeostasis and endolysosomal function in hypothalamic neurons

Ana Cristina Reguera · Cristina Miralpeix · Maribel Bernard · Sebastián Zagmutt · Montserrat Bolaños-Hurtado · Carlos Palacín · Andrea Fuentes · María Rodríguez-García · Anna Fosch · Jesús Garcia-Chica · Ramon Barnadas-Rodríguez · Nermeen Fawzy · Robert Zimmermann · Emily Eden · Núria Casals · Rosalía Rodríguez-Rodríguez

Received: 13 May 2026 / Revised: 4 September 2026 / Accepted: 6 September 2026
© The Author(s) 2026

Abstract

The endolysosomal system is central to neuronal homeostasis, yet how nutrient sensing regulates endolysosomal lipids remains poorly understood. Bis(monoacylglycerol)phosphate (BMP), a signature phospholipid of late endosomes, is required for intraluminal vesicle formation, cholesterol handling, and lysosomal function, but the mechanisms preserving neuronal BMP homeostasis are largely unknown. Here, we identify a nutrient-sensitive pathway linking metabolic state to BMP homeostasis in hypothalamic neurons. We show that the neuronal lipid sensor carnitine palmitoyltransferase 1C (CPT1C) restrains the BMP hydrolase ABHD6. Loss of CPT1C increases ABHD6 activity, lowers intracellular BMP levels, and impairs endosomal maturation, extracellular vesicle release, and lysosomal acidification and proteolytic activity. Acute ABHD6 inhibition restores BMP levels in CPT1C-deficient neurons, indicating that BMP depletion results primarily from enhanced hydrolysis. Lipid overload similarly increases ABHD6 activity and lowers BMP levels in wild-type neurons and hypothalamus, whereas CPT1C-deficient cells and mice display constitutively elevated ABHD6 activity and fail to further adapt to lipid excess. Together, these findings identify CPT1C as a nutrient-sensitive regulator of neuronal BMP homeostasis and endolysosomal function.

Keywords CPT1C · ABHD6 · Bis(monoacylglycerol)phosphate (BMP) · Endolysosomal system · Neurons

Introduction

The endolysosomal system plays a pivotal role in neuronal homeostasis and has emerged as a key node in the pathophysiology of several neurological and metabolic diseases [1, 2]. Endosomes and lysosomes are highly specialized organelles that integrate nutrient sensing, cargo degradation, membrane trafficking, and lipid metabolism,

This Article in Press is shared early to give you faster access to new research. It is citable and carries a permanent DOI. The final edited version will replace it automatically.

https://doi.org/10.1007/s00018-026-06451-3

Published online: 07 October 2026

and their function is particularly sensitive to metabolic stress [3–5]. How neuronal metabolic state is coupled to endolysosomal function, however, remains poorly understood.

A key determinant of endolysosomal identity is bis(monoacylglycero)phosphate (BMP), originally named lyso-bis-phosphatidic acid (LBPA), an atypical phospholipid enriched in the intraluminal vesicles (ILVs) of late endosomes (LEs), in contrast to other phospholipids that distribute broadly across endocytic and secretory membranes [6]. BMP supports late endosome maturation, ILV organization, cholesterol handling, and lysosomal degradative capacity [7, 8]. Altered BMP levels have been reported in lysosomal storage disorders, neurodegeneration, ageing, and more recently in metabolic diseases such as obesity, highlighting BMP as both a functional component and a readout of endolysosomal dysfunction in the context of these diseases [9–15]. Alterations in BMP abundance or turnover disrupt endolysosomal dynamics and contribute to phospholipidosis and other metabolic pathologies [11, 16, 17]. Although nutrient availability is known to modulate lysosomal function, chronic exposure to excessive lipids, such as during high-fat diet (HFD) intake, impairs endolysosomal activity [18–20]. Despite this growing interest, the mechanisms that maintain BMP homeostasis in neurons are poorly defined, and how nutrient-sensing pathways specifically regulate BMP metabolism in neurons has not yet been elucidated.

Recent studies have identified the enzymatic machinery governing BMP homeostasis. Among the known BMP hydrolases, α/β-hydrolase domain-containing 6 (ABHD6) has emerged as a major contributor, accounting for a substantial fraction of BMP hydrolase activity in brain and liver [12, 21]. ABHD6 was first characterized as a monoacylglycerol hydrolase in the endocannabinoid system but is now recognized as a multifunctional lipid hydrolase with important roles in energy balance and nutrient sensing [22–24]. However, important mechanistic questions remain unresolved. While ABHD6 is localized to the cytosolic side of membranes, BMP resides predominantly in the lumen of LEs, suggesting that hydrolysis may occur after ILV back-fusion with the limiting membrane [21, 25]. Furthermore, although ABHD6 has been implicated in hypothalamic energy regulation and nutrient sensing [26–28], the mechanisms coupling its BMP hydrolase activity to metabolic state in neurons and nutritional cues remain unclear.

Carnitine palmitoyltransferase 1 C (CPT1C), a neuron-specific isoform of the CPT1 family, is a key regulator of neuronal energy homeostasis and lipid metabolism [29, 30]. Unlike its mitochondrial counterparts, CPT1C predominantly localizes to the endoplasmic reticulum (ER) and endosomal membranes, where it modulates neuronal growth, vesicular trafficking, and responses to nutrient availability [31, 32]. We previously identified CPT1C as the first protein regulator of ABHD6 activity in hypothalamic neurons and demonstrated CPT1C-ABHD6 interaction [28]. CPT1C acts as a negative modulator of ABHD6 hydrolase activity in a nutrient-dependent manner, influencing endocannabinoid signaling and ABHD6 activity in hypothalamic neurons and hypothalamic tissue from fed and fasted mice [28]. These observations raised the possibility that CPT1C could couple nutrient sensing to ABHD6-dependent control of BMP homeostasis and further endolysosomal function in neurons. Moreover, although CPT1C is known to affect late endosome–lysosome dynamics and neuronal lipid handling, whether this role involves regulation of ABHD6-mediated BMP degradation had not been investigated.

Here, we hypothesize that the CPT1C–ABHD6 axis constitutes a nutrient-regulated mechanism controlling BMP homeostasis and endolysosomal functionality in neurons, particularly in the context of lipid overload. To test this, we generated a CPT1C-deficient hypothalamic neuronal model using CRISPR-Cas9 and examined the consequences of CPT1C loss on BMP levels and BMP-dependent functions under basal and fatty-acid exposure. We complemented these experiments with in vivo analyses of BMP metabolism in wild-type (WT) and CPT1C KO mice subjected to a high-fat diet (HFD). Our results demonstrate that loss of CPT1C results in BMP depletion, impaired endosomal maturation, reduced small extracellular vesicle (EV) release, and defective lysosomal acidification and activity. Moreover, lipid overload increases ABHD6 activity and lowers BMP levels in wild-type neurons and hypothalamus, whereas CPT1C-deficient neurons and mice display constitutively elevated ABHD6 activity and a blunted adaptive response. These findings identify a nutrient-sensitive mechanism linking neuronal metabolic state to BMP homeostasis and endolysosomal competence.

Methods

Cell lines and culture conditions

HEK293T (RRID: CVCL_0063) and hypothalamic neuronal GT1-7 cells (RRID: CVCL_0281) were maintained under standard culture conditions. HEK293T cells were maintained in high-glucose DMEM (Sigma-Aldrich) containing 10% FBS (Sigma-Aldrich), 1% penicillin–streptomycin (Sigma-Aldrich), and 1% glutamine (Lab-clinics). GT1-7 cells were maintained in high-glucose DMEM supplemented with sodium pyruvate, 10% FBS, 1% penicillin–streptomycin, and 1% glutamine. Cell cultures were incubated at 37 °C in a humidified atmosphere of 5% CO_2. All cells were passed before reaching complete confluence and were regularly tested for mycoplasma contamination.

CRISPR/Cas9-mediated genome editing of mouse hypothalamic neuronal GT1-7 cells

sgRNA design and plasmid construction

The CRISPR/Cas9 system was used to generate CPT1C-knockout (CPT1C-KO) GT1-7 hypothalamic neuronal cells. Candidate sgRNAs targeting different exons of the mouse *Cpt1c* gene were designed using Benchling database based on the corresponding genomic sequence (Gene ID: ENSMUSG00000007783). The selected 20-nt guide sequences targeted exons 1, 6, 9, and 10 and were as follows: exon 1, 5′-GTTTGTGGACTCATTACAC G-3′; exon 6, 5′-CATTTGCCAGCGCTGTAGCG-3′; exon 9, 5′-GAACATCCTCTCATACTGGG-3′; and exon 10, 5′-CACGTGGCTGTCTTCCACCG-3′. Each sgRNA was cloned into the lentiCRISPR v2 vector (Addgene #52961) following the previously described protocol [33]. The resulting constructs were transformed into *E. coli* DH5α competent cells by heat shock and plated on LB agar supplemented with ampicillin, followed by overnight incubation at 37 °C. Single colonies were inoculated into LB medium containing ampicillin and grown overnight at 37 °C with shaking. Plasmids were isolated using the NucleoSpin TriPrep kit (Thermo Fisher) according to the manufacturer's instructions and verified by Sanger sequencing using the U6-Fwd primer (5′-GAGGGCCTATTT CCCATGATTCC-3′).

Lentiviral production and transduction

Lentiviral particles were produced by co-transfecting HEK293T cells with the sgRNA-lentiCRISPR construct and the packaging plasmids psPAX2 and pMD2.G (Addgene) using a standard calcium-phosphate transfection protocol. Cells were incubated for 48 h to allow viral production, after which the culture supernatant was collected, filtered, and concentrated to obtain viral particles. The harvested lentiviral particles were used to transduce GT1-7 cells. Functional viral titers were estimated by serial dilution in GT1-7 cells followed by puromycin selection. Transduction efficiency was assessed based on cell survival after selection in medium containing 0.5 µg/ml puromycin (InvivoGen). Loss of CPT1C expression in puromycin-resistant cells was confirmed by western blotting. Among the sgRNAs tested, the guide targeting exon 6 showed the highest efficiency in reducing CPT1C protein levels (Supplementary Fig. 1) and was therefore selected for generation of the final CPT1C-KO GT1-7 cell line.

Preparation of fatty acid-BSA complexes

Palmitate-BSA and oleate-BSA complexes were prepared as previously described, with minor modifications [34]. Briefly, palmitic acid and oleic acid (Sigma-Aldrich) were dissolved separately in 0.1 M NaOH to obtain 30 mM stock solutions and heated at 80 °C for 5 min under stirring. Fatty acid-free BSA (Merck Millipore) was dissolved in 0.9% NaCl at 100 mg/ml at 37 °C. Fatty acid stock solutions were then mixed with the prewarmed BSA

solution to obtain 3 mM fatty acid-BSA complexes and incubated for at least 5 min at 37 °C to allow complex formation. A BSA-only control solution was prepared in parallel using the same fatty acid-free BSA solution and vehicle, but without added fatty acid. Solutions were then passed through a 0.45 µm syringe filter, aliquoted, and stored at −20 °C until use. Before cell treatment, stock solutions were warmed to 37 °C and diluted in treatment culture medium, consisting of completed DMEM but supplemented 1% FBS, to a final fatty acid concentration of 300 µM. WT and CPT1C-KO GT1-7 cells were pre-incubated for 1 h in the same treatment medium and were then exposed for 16 h to fatty acid-BSA complexes.

PG supplementation for cellular BMP enrichment

PC and PG liposomes were used for cellular BMP enrichment experiments based on previous studies [35, 36]. Soy phosphatidylcholine (PC 95%, Avanti Polar Lipids) and 1,2-dioleoyl-sn-glycero-3-phospho-(1'-rac-glycerol) (DOPG, Avanti Polar Lipids) were dissolved separately in chloroform:methanol (2:1, v/v), dried by rotary evaporation to form a thin lipid film, and vacuum-dried overnight. The resulting lipid films were rehydrated in PBS and agitated for 30 min to facilitate lipid resuspension. Liposome suspensions were subsequently extruded through a 200 nm membrane. Liposomes were then diluted in culture medium and added to cells at a final concentration of 100 µM for 24 h. PC liposomes were used as control, whereas PG liposomes were used for BMP enrichment.

ABHD6 hydrolase activity assay

Cell and tissue processing

ABHD6 hydrolase activity was measured using the 4-methylumbelliferyl-heptanoate (4-MUH)-based fluorogenic assay, as previously described [28]. For endogenous ABHD6 activity measurements in cell homogenates, WT and CPT1C-KO cells were harvested 48 h after seeding, washed once with PBS, pelleted (3,200 rpm, 5 min), briefly frozen at −80 °C for 10 min, resuspended in 100 µl Tris–EDTA buffer (50 mM Tris–HCl, 1 mM EDTA, pH 7.4), and briefly sonicated. The same procedure was applied to WT and CPT1C-KO GT1-7 cells after treatment with BSA, palmitic acid (PA), or oleic acid (OA) (300 µM, 24 h). For the substrate competition assay, HEK293T cells were transiently transfected with cDNA encoding ABHD6-YFP using FuGENE HD (Promega), according to the manufacturer's instructions. Cells were harvested 48 h after transfection and processed as described above. For endogenous ABHD6 activity measurements in tissue homogenates, hypothalamus, hippocampus, and liver were rapidly dissected and maintained at 4 °C, dounce-homogenized in 200 µl Tris–EDTA buffer (50 mM Tris–HCl, 1 mM EDTA, pH 7.4), and briefly sonicated. Protein concentration in cell and tissue homogenates was determined before the assay using the Pierce™ BCA Protein Assay Kit (Thermo Fisher Scientific), according to the manufacturer's instructions.

ABHD6-based 4-MUH activity assay

The assay was performed in black 96-well plates in a final volume of 100 µl per well, using 0.1 µg total protein for liver homogenates and 1 µg total protein for cell and brain homogenates. To determine endogenous ABHD6 activity, homogenates were pre-incubated for 30 min at 37 °C with either the selective ABHD6 inhibitor WWL70 (10 µM; Cayman Chemical) or vehicle (DMSO), and the reaction was initiated by addition of 4-MUH (Sigma-Aldrich) to a final concentration of 50 µM. Fluorescence (λ_{ex} 355 nm/λ_{em} 460 nm) was measured at 37 °C every 10 min for 90–120 min using a Synergy H1 microplate reader (BioTek). ABHD6-specific activity was calculated by subtracting the signal obtained in the presence of WWL70 from that obtained in vehicle-treated samples. A 4-methylumbelliferone (4-MU; Sigma-Aldrich) standard curve was used for quantification, and activity was expressed as nmol 4-MU/mg. For substrate competition assays, homogenates from ABHD6-overexpressing HEK293T cells were pre-incubated with bis(monoacylglycero)phosphate (BMP; final concentration 0–500 µM;

Avanti Polar Lipids) for 30 min at 37 °C before addition of 4-MUH. Fluorescence was then recorded under the same conditions as described above.

Protein extraction and Western blotting

For protein extraction from cultured cells or EVs, samples were collected in lysis buffer (20 mM Tris–HCl (pH 7.4), 5 mM EDTA, 1% NP-40, 150 mM NaCl) supplemented with protease and phosphatase inhibitors (Thermo Fisher Scientific) and incubated on ice for 1 h. For protein extraction from tissues, samples were homogenized in the same lysis buffer in a FastPrep®−24 Homogenizer (MP Biomedicals). Lysates were clarified by centrifugation at 10,000 × g for 15 min at 4 °C, and protein concentration was determined using the Pierce™ BCA Protein Assay Kit (Thermo Fisher Scientific). Western blots were carried out as previously described [34]. Briefly, whole cell lysates were eluted with 1 × SDS sample buffer. Protein extracts were heated for 5 min at 95ºC, separated on 10% SDS–PAGE, and transferred into PVDF membranes. Proteins were probed with antibodies against: rabbit anti-CPT1C produced in our laboratory (1/6000) [28], rabbit anti-ABHD6 (1/1000; Cell Signaling Technology, #97,573), mouse anti-β-actin (1/10,000; Thermo Fisher Scientific, #MA1-91,399), mouse anti-Alix (1/1,000; Cell Signaling Technology, #2171), rabbit anti-Flotillin-1 (1/2,000; Santa Cruz Biotechnology, #sc-25506), and rabbit anti-Calnexin (1/1000; Abcam, #ab22598). Each membrane was then incubated with the corresponding secondary antibody and developed using Immobilon Forte Western HRP substrate (Merck Millipore). Images were captured using a ChemiDoc™ Imaging System (Bio-Rad). Band intensity was quantified by densitometry with Image Lab software (Bio-Rad). Protein levels were normalized to the corresponding loading control and, when applicable, to the control group.

BMP immunofluorescence and filipin staining

WT and CPT1C-KO GT1-7 cells were seeded onto poly-L-lysine-coated coverslips and allowed to adhere for 24 h. When indicated, cells were subjected to the corresponding treatments before fixation and staining. For BMP/LBPA immunostaining, cells were incubated with CellTracker™ Green CMFDA (Thermo Fisher Scientific) for 30 min and then fixed in cold 4% PFA for 15 min. Fixed cells were permeabilized with 0.05% saponin for 15 min at room temperature and incubated with mouse anti-LBPA primary antibody (1/1000; Sigma-Aldrich, #MABT837) followed by Alexa Fluor 633-conjugated anti-mouse secondary antibody (1/1000; Invitrogen, #A-21052). Nuclei were counterstained with Hoechst (Sigma-Aldrich), and coverslips were mounted using Fluoromount-G® anti-fade mounting medium (Southern Biotech). For free cholesterol staining, fixed cells were incubated with filipin (Sigma-Aldrich) (0.05 mg/ml for 2 h). Images were acquired using a Leica DMi8 confocal microscope (Leica Microsystems) with a 63 × objective and analyzed using Fiji (ImageJ, NIH). BMP mean fluorescence intensity was expressed as fluorescence intensity per cell by normalizing the BMP signal to the CellTracker-positive area of each individual cell. Filipin mean fluorescence intensity was expressed as fluorescence intensity per cell, normalized to the area of each individual cell.

Cellular cholesterol quantification

Cellular total cholesterol content was quantified using the Amplex Red Cholesterol Assay Kit (Thermo Fisher Scientific). WT and CPT1C-KO GT1-7 cells were seeded at the same initial density and collected at comparable confluence. Cells were washed with PBS, and lipids were extracted using hexane: isopropanol (3:2, v/v). The organic phase was collected and evaporated to dryness before processing according to the manufacturer's instructions. Fluorescence was measured using a microplate reader at the excitation/emission wavelengths recommended by the manufacturer. Cholesterol concentration was calculated from a cholesterol standard curve and normalized to total protein content determined from matched samples using the Pierce™ BCA Protein Assay Kit (Thermo Fisher Scientific).

Immunofluorescence and colocalization analysis

Colocalization analyses of CPT1C and ABHD6 with each other and with organelle markers were performed in HeLa cells transiently expressing tagged CPT1C and/or ABHD6 constructs. HeLa cells were seeded onto poly-L-lysine-coated glass coverslips. The following day, cells were transfected with plasmids encoding CPT1C-EGFP and/or ABHD6-mCherry using FuGENE HD transfection reagent, according to the manufacturer's instructions, and then fixed with 4% PFA.

For ER and LE/lysosomal colocalization analyses, fixed and permeabilized cells were then incubated with primary antibodies against calnexin (1/2000; Abcam, #ab22595), as an ER marker, or LAMP1 (1/1000; Sigma-Aldrich, #L1418), as a LE/lysosomal marker, followed by incubation with the corresponding Alexa Fluor-conjugated secondary antibodies, as indicated. For BMP/LBPA colocalization analyses, cells expressing CPT1C-EGFP or ABHD6-mCherry were immunostained with anti-BMP/LBPA antibody. In parallel, non-transfected HeLa cells were co-immunostained for LAMP1 and BMP/LBPA to assess the overlap between BMP-positive and LE/lysosomal compartments. After each antibody incubation, coverslips were washed with PBS and mounted using Fluoromount-G antifade mounting medium. Confocal images were acquired using a Leica DMi8 confocal microscope with a 63 × objective. Image acquisition settings were kept constant within each experiment. Colocalization was quantified using Fiji/ImageJ and expressed as Manders' overlap coefficient. For BMP colocalization analyses, the M2 Manders coefficient was calculated as the fraction of BMP signal overlapping with CPT1C, ABHD6 or LAMP1.

Analysis of lysosomal compartment and function

Lysosomal compartments and function were assessed using complementary fluorescence-based assays. LysoTracker Red DND-99 (Thermo Fisher Scientific), a cell-permeable fluorescent dye that accumulates in acidic organelles, was used to evaluate the acidic lysosomal compartment. The Magic Red kit (Immunochemistry Technologies), which uses a cell-permeable fluorogenic substrate that releases membrane-impermeable fluorescent cresyl violet upon hydrolysis by active cathepsin B, was used to assess lysosomal cathepsin B activity [19]. For these experiments, WT and CPT1C-KO GT1-7 cells were seeded onto poly-L-lysine-coated coverslips in 24-well plates and incubated with either 50 nM LysoTracker Red DND-99 or Magic Red Cathepsin B substrate (1/250 dilution) for 45 min at 37 °C. Cells were then fixed in cold 4% PFA for 15 min, counterstained with Hoechst (Sigma-Aldrich), and mounted with Fluoromount-G® antifade mounting medium. Images were acquired using a Leica DMi8 confocal microscope (Leica Microsystems) with a 63 × objective and analyzed using Fiji (ImageJ, NIH). LysoTracker mean fluorescence intensity, LysoTracker-positive area, the number of LysoTracker-positive puncta per cell, and the distance of these puncta from the nucleus were quantified as measures of the acidic lysosomal compartment, whereas Magic Red mean fluorescence intensity was quantified as a measure of lysosomal cathepsin B activity.

Lysosomal pH was assessed in live cells using LysoSensor Yellow/Blue DND-160 (Thermo Fisher Scientific), a ratiometric fluorescent dye that exhibits a pH-dependent shift from blue to yellow fluorescence as acidity increases. WT and CPT1C-KO GT1-7 cells were seeded in 8-well microscopy chambers (μ-slide 8 Well; Ibidi). After 24 h, cells were incubated with 1 μM LysoSensor Yellow/Blue DND-160 for 5 min at 37 °C and imaged immediately under live-cell conditions. Fluorescence was acquired using UV excitation with two emission channels corresponding to the blue and yellow signals. Images were acquired using a Leica DMi8 confocal microscope and analyzed using Fiji as described. The yellow-to-blue emission ratio was calculated as the ratio of background-subtracted fluorescence intensity in the yellow channel to that in the blue channel and used as a readout of lysosomal acidification.

Transmission electron microscopy (TEM)

Endosome morphology in WT and CPT1C-KO GT1-7 cells was assessed by TEM [37]. Cells were seeded onto poly-L-lysine-coated coverslips in 24-well plates. Twenty-four hours after seeding, cells were fixed in 2% paraformaldehyde/2% glutaraldehyde in 0.1 M sodium cacodylate buffer for 30 min at room temperature, post-fixed in 1% osmium tetroxide/1.5% potassium ferricyanide for 1 h on ice and incubated with UA-Zero for 1 h at room temperature in the dark. Samples were then dehydrated through a graded ethanol series and embedded in TAAB 812 resin. Resin blocks were polymerized overnight at 65 °C. Ultrathin Sects. (70 nm) were cut using a Leica EM UC6 ultramicrotome (Leica Microsystems) and imaged on a JEOL JEM-1400Plus transmission electron microscope (JEOL Ltd.). Endosomes were identified based on the presence of intraluminal vesicles (ILVs), and endosome maturation was inferred from ILV density. Endosomal area was quantified from TEM images using Fiji (ImageJ, NIH).

Isolation of small EV- enriched fraction by sequential ultracentrifugation and analysis

EVs were isolated from serum-free conditioned medium collected from WT and CPT1C-KO GT1-7 cells maintained under basal conditions for 24 h by sequential ultracentrifugation, based on the protocol previously described [38]. Briefly, conditioned medium was collected and centrifuged at 300 × g for 5 min at room temperature to remove cells, followed by centrifugation at 2,500 × g for 20 min at 4 °C to eliminate cell debris and apoptotic bodies. The resulting supernatant was then centrifuged at 10,000 × g for 30 min at 4 °C to remove large microvesicles. Subsequently, the supernatant was ultracentrifuged at 100,000 × g for 2 h at 4 °C. The pellet was washed once with 1 × PBS and ultracentrifuged again at 100,000 × g for 1 h at 4 °C. The final pellet, corresponding to the small EV-enriched fraction, was resuspended according to the downstream application. For protein analysis, EV pellets were resuspended in a lysis buffer, whereas for nanoparticle tracking analysis (NTA), EV pellets were resuspended in 1 × PBS. EV size distribution and particle concentration were measured using a NanoSight NS300 instrument (Malvern Panalytical). EVs were resuspended in 1 × PBS and diluted to the working range of the system (1 × 10^6 to 1 × 10^9 particles/ml). Videos were recorded and analyzed with the NanoSight NS300 software (version 3.4) using a sCMOS camera.

Animals and sample collection

Male CPT1C-KO mice (8–10 weeks old) and their WT littermates with the same genetic background (C57BL/6 J) were used for the experiments. Animals were housed under a 12 h light/12 h dark cycle (lights on at 8 a.m. and off at 8 p.m.) in a temperature- and humidity-controlled room and were allowed free access to water and standard laboratory chow diet. For the dietary intervention, mice were randomly assigned to receive either a standard diet (SD, 10% kcal from fat, D12450J) or a high-fat diet (HFD, 60% kcal from fat, D12492) (Research Diets) for 7 days. Animals were euthanatized and hypothalamus, hippocampus, and liver were rapidly collected for downstream analyses. All animal procedures were performed in agreement with European guidelines (2010/63/EU) and approved by the Ethical Committee of the University of Barcelona (n.10906 and n. 10,210 from the Generalitat de Catalunya). All efforts were made to minimize animal suffering and to minimize the number of animals used. Animal studies are reported in compliance with the ARRIVE guidelines.

Targeted BMP analysis

Targeted BMP analysis was performed in hypothalamus, hippocampus, and liver samples from WT and CPT1C-KO mice after 7 days of SD or HFD feeding. Lipids were extracted using a modified version of the method previously described [39]. Samples were extracted using 1 mL MTBE/MeOH (3:1, v/v) containing 500 pmol butylated hydroxytoluene (BHT), 0.01% acetic acid, and 150 pmol internal standards (14:0–14:0 BMP) per

sample. Extraction was carried out under constant shaking on a thermomixer at 1,200 rpm for 30 min at room temperature. Subsequently, 200 µl ddH2O was added, followed by incubation for 10 min at room temperature. Samples were then centrifuged at 20,000 × g for 5 min at room temperature to induce phase separation. The upper organic phase was collected, dried under a stream of nitrogen, and reconstituted in MeOH/2-propanol/ultrapure water (6:3:1, v/v/v) for UPLC–MS analysis.

BMP species were detected on an Agilent 6470 triple-quadrupole mass spectrometer equipped with Agilent Jet Stream ESI (Agilent Technologies, Santa Clara, CA) under fast polarity switching, with simultaneous acquisition in positive and negative ion modes in a single run, controlled by Agilent MassHunter Acquisition software (version 10.1). BMP species were analyzed in dynamic multiple reaction monitoring (dMRM) mode. In negative ion mode, BMP species were monitored as $[M–H]^-$ to fatty-acid anion transitions, using a collision energy of 35 V. In positive ion mode, BMP species were monitored as $[M+NH_4]^+$ to monoacylglycerol (MG) fragment transitions, acquired at unit resolution using a collision energy of 25 V. Because BMP-specific MG fragments showed lower sensitivity, quantification relied on negative-mode fatty-acid anion transitions and analyte-to-internal-standard ratios, whereas positive-mode MG fragments were used as qualifier transitions.

Discrimination between BMP and phosphatidylglycerol (PG) was validated during method development using commercially available pure standards, separate external calibration curves, and spike-in experiments in lipid extracts. The standards used included 14:0/14:0 BMP and 18:1/18:1 BMP for BMP, and 17:0/17:0 PG and 18:1/18:1 PG for PG. BMP and PG species were baseline separated under the reverse-phase UPLC conditions used, and endogenous species followed the expected equivalent carbon number (ECN) retention behavior. In addition, BMP and PG showed distinct MS/MS fragmentation behavior in positive ion mode, with BMP generating MG fragments and PG generating diacylglycerol (DG) fragments. PG species were monitored during method validation using $[M–H]^-$ to fatty-acid anion transitions in negative ion mode and DG qualifier fragments in positive ion mode, using collision energies of 45 V and 15 V, respectively. Final BMP assignments therefore integrated chromatographic retention-time separation, comparison with pure standards, spike-in confirmation, ECN-consistent retention behavior, dMRM transitions, and BMP-specific qualifier fragmentation.

The targeted BMP panel included BMP 34:0, BMP 34:1, BMP 34:2, BMP 36:0, BMP 36:1, BMP 36:2, BMP 36:3, BMP 38:4, BMP 38:5, BMP 38:6, BMP 40:5, BMP 40:7, BMP 40:8, BMP 42:8, BMP 42:10, BMP 44:10, BMP 44:11, and BMP 44:12. Total BMP was calculated as the sum of the annotated BMP molecular species included in the targeted panel. Data processing was performed with Agilent MassHunter Quantitative Analysis software version 10.1 and Agilent MassHunter Qualitative Analysis software version 10.0. Concentrations were calculated using analyte/internal-standard ratios and external calibration with BMP 36:2 (Avanti Polar Lipids), and results were expressed as nmol/g tissue.

Statistical analysis

Data processing and statistical analyses were performed using GraphPad Prism 10.0. Data are presented as mean ± SD of biologically independent replicates. The number of biologically independent replicates (n) is indicated in the corresponding figure legends. Comparisons between two groups were performed using Student's *t*-test. Grouped comparisons were analyzed by two-way ANOVA followed by Bonferroni's post hoc test. A P value < 0.05 was considered statistically significant.

Results

CPT1C restrains ABHD6-dependent BMP homeostasis in hypothalamic neurons

To investigate whether CPT1C regulates BMP homeostasis through ABHD6 in hypothalamic neurons, we used the mouse GT1-7 cell line, which endogenously expresses both CPT1C and ABHD6 [28]. We generated CPT1C-KO

GT1-7 cells using CRISPR-Cas9 and first validated the model by measuring ABHD6 activity. Consistent with our previous work, ABHD6 activity, determined using a 4-methylumbelliferyl heptanoate (4-MUH) hydrolysis assay, was significantly increased in CPT1C-KO cells compared WT cells (Fig. 1A,B; Supplementary Fig. 1), whereas total ABHD6 protein levels were unchanged (Fig. 1C-E). Thus, loss of CPT1C enhances ABHD6 activity in hypothalamic neurons without altering ABHD6 expression.

Because ABHD6 has been identified as a BMP hydrolase [12], we next examined whether CPT1C deficiency affected cellular BMP levels. In a substrate competition assay performed in ABHD6-overexpressing cells, increasing BMP concentrations dose-dependently reduced 4-MUH hydrolysis (Supplementary Fig. 2A), supporting ABHD6 activity toward BMP. Immunocytochemical analysis revealed that CPT1C-KO cells contained significantly less BMP than WT cells (Fig. 1F,G). Importantly, acute pharmacological inhibition of ABHD6 with WWL70 restored BMP levels in CPT1C-KO cells (Fig. 1H,I), indicating that BMP depletion in the absence of CPT1C results primarily from enhanced ABHD6-dependent hydrolysis.

To exclude the possibility that reduced BMP levels were caused by defective biosynthesis rather than enhanced degradation, we supplemented cells with PG, the immediate precursor of BMP, using phosphatidylcholine (PC) as a control [36]. PG supplementation increased BMP levels in both WT and CPT1C-KO cells to a similar extent (Supplementary Fig. 3), indicating that the capacity to generate BMP is preserved in CPT1C-deficient cells. These findings support a model in which CPT1C maintains BMP homeostasis mainly by limiting ABHD6-dependent BMP degradation.

To further assess whether the CPT1C-ABHD6-BMP axis is spatially compatible with regulation at endolysosomal interfaces, we performed confocal colocalization analyses in HeLa cells transiently expressing tagged CPT1C and/or ABHD6 constructs. HeLa cells were selected for these experiments because they allow efficient transient transfection and robust visualization of CPT1C-EGFP and ABHD6-mCherry. Consistent with previous reports on CPT1C subcellular localization [31, 32]. CPT1C-EGFP showed localization compatible with the ER marker calnexin. ABHD6-mCherry also showed partial overlap with calnexin, and co-expression of CPT1C-EGFP and ABHD6-mCherry revealed partial colocalization between both proteins (Supplementary Fig. 4).

We next examined the relationship of CPT1C and ABHD6 with LE/lysosomal and BMP-positive compartments. Both CPT1C-EGFP and ABHD6-mCherry showed partial colocalization with the LE/lysosomal marker LAMP1. In addition, both proteins partially overlapped with BMP-positive structures, while LAMP1-BMP colocalization was included as a reference for BMP-enriched LE/lysosomal compartments (Supplementary Fig. 5). These data support the spatial compatibility of the CPT1C-ABHD6-BMP regulatory axis and suggest that CPT1C and ABHD6 are positioned in proximity to BMP-containing endolysosomal compartments.

Given the close relationship between BMP and endolysosomal cholesterol handling [35, 40], we therefore assessed intracellular free cholesterol by filipin staining and found significantly reduced cholesterol levels in CPT1C-KO cells relative to WT cells (Fig. 1J,K), consisting with the reduction in BMP. Since filipin staining provides a semi-quantitative readout of intracellular free cholesterol, we complemented this analysis with a biochemical quantification of total cellular cholesterol using an Amplex Red-based enzymatic assay after lipid extraction. In agreement with the filipin staining results, CPT1C-KO cells showed significantly lower total cholesterol content than WT cells (Supplementary Fig. 6). These biochemical data corroborate the imaging results and support the conclusion that CPT1C deficiency is associated with reduced cellular cholesterol abundance and altered cholesterol homeostasis in hypothalamic neurons.

To assess whether CPT1C deficiency led to lysosomal accumulation of free cholesterol, we performed Filipin/LAMP1 co-staining and quantified the fraction of filipin signal overlapping with LAMP1-positive compartments. CPT1C-KO cells did not show increased filipin accumulation in LAMP1-positive compartments; rather, filipin-LAMP1 overlap was significantly reduced compared with WT cells (Supplementary Fig. 7).

Together, these results identify CPT1C as a regulator of BMP homeostasis in hypothalamic neurons through functional modulation of ABHD6 hydrolase activity. Loss of CPT1C leads to increased ABHD6 activity, increased BMP degradation, and a concomitant reduction in both BMP and intracellular cholesterol levels.

https://doi.org/10.1007/s00018-026-06451-3

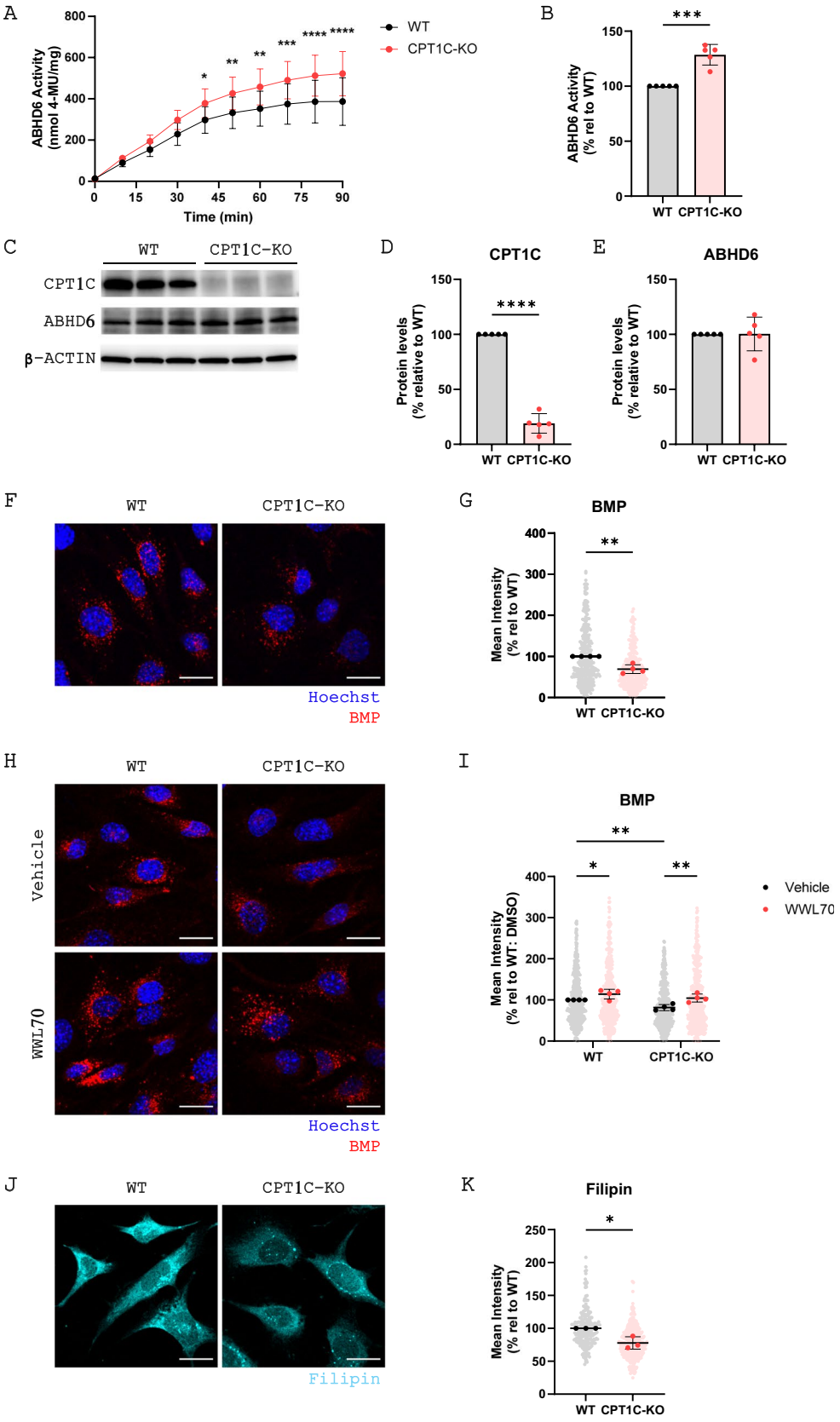


Fig. 1 ABHD6 activity, BMP levels and intracellular cholesterol in WT and CPT1C KO GT1-7 cells. A-B) Kinetics (**A**) and quantification (**B**) of ABHD6 activity in WT and CPT1C-KO cells. Quantification of ABHD6 activity was calculated from the AUCs of WT and CPT1C-KO cells (n = 5 independent experiments). Data are shown as mean ± SD. **C**) Representative image from immunoblotting of CPT1C, ABHD6 and β-actin in WT and CPT1C-KO cells. D-E) Immunoblot quantification of CPT1C and ABHD6 (n = 5 independent experiments). Data are shown as mean ± SD. F) Representative confocal images of BMP immunocytochemistry in WT and CPT1C-KO cells. Scale bars = 20 µm. G) Quantification of BMP levels per cell in WT and CPT1C-KO cells (n = 4 independent experiments). Data are shown as mean ± SD. H) Representative confocal images of BMP immunocytochemistry in WT and CPT1C-KO cells treated with DMSO (vehicle) or 10 µM WWL70 for 4 h. Scale bars = 20 µm. I) Quantification of BMP levels per cell in WT and CPT1C-KO cells after treatment with WWL70 for 4 h (n = 4 independent experiments). Data are shown as mean ± SD. J) Representative confocal images of Filipin staining in WT and CPT1C-KO cells. Scale bars = 20 µm. K) Quantification of Filipin levels per cell in WT and CPT1C-KO cells (n = 3 independent experiments). Data are shown as mean ± SD

CPT1C deficiency impairs endosomal maturation and reduces EV release in hypothalamic neurons

BMP is highly enriched in ILVs of LEs and is required for LE maturation and endolysosomal membrane organization [21]. We therefore explored whether CPT1C deficiency and its reduced BMP homeostasis was associated with altered endosomal morphology and maturation. Transmission electron microscopy (TEM) analysis revealed a marked shift in endosomal type in CPT1C-KO cells. Based on ILV density, endosomal structures were classified as early endosomes (EEs) or LEs (Fig. 2A), and the relative proportion of each category within the EE+LE population was quantified per independent experiment. CPT1C-KO cells displayed a higher proportion of EE profiles and a lower proportion of LE profiles compared with WT cells (Fig. 2B), consistent with altered endosomal maturation. Because TEM fields did not consistently contain complete cell profiles, this analysis was expressed as the relative distribution of EE and LE profiles per independent experiment rather than as number of structures per cell.

In addition to this shift in endosomal profile distribution, endosomal organelles in CPT1C-KO cells were generally smaller. Quantification of organelle areas showed a trend toward reduced size of EEs, LEs, and endolysosomal structures compared with WT cells (Fig. 2C-E). These changes are consistent with impaired endosomal maturation in the absence of CPT1C.

Because ILVs within LEs give rise to exosomes, defective endosomal maturation is often accompanied by altered EV release. We therefore isolated EVs from conditioned media by sequential ultracentrifugation. Nanoparticle tracking analysis and immunoblotting confirmed enrichment of a small EV fraction, with the expected size range (50–500 nm) and expression of EV markers including Flotillin-1 and Alix, together with depletion of calnexin relative to input lysate (Supplementary Fig. 8). CPT1C-KO cells released significantly fewer EVs than WT cells (Fig. 2F), whereas EV size distribution was unchanged and particle size was lower than 150 nm in both genotypes (Fig. 2G), indicating that CPT1C deficiency primarily affects small EV output rather than EV size. Thus, CPT1C is required for efficient endosomal maturation and normal small EV release in hypothalamic neurons.

CPT1C is required for lysosomal acidification and proteolytic activity

Given the structural defects observed in the endolysosomal system of CPT1C-KO cells, we next assessed whether lysosomal function was also altered. LysoTracker staining revealed a marked reduction in fluorescence intensity and LysoTracker-positive area in CPT1C-KO cells compared with WT cells (Fig. 3A-C), consistent with a smaller and less acidic endolysosomal compartment. To further determine whether this phenotype reflected changes in the number or intracellular distribution of acidic compartments, we performed additional quantitative analyses of LysoTracker-positive puncta. CPT1C-KO cells did not show a significant change in the number of LysoTracker-positive puncta compared with WT cells (Supplementary Fig. 9A). In addition, analysis of the distance between LysoTracker-positive puncta and the nucleus showed no significant difference between genotypes, indicating that CPT1C deficiency did not cause a major redistribution of LysoTracker-positive compartments relative to the nucleus (Supplementary Fig. 9B).

To corroborate the reduction in lysosomal acidity, we used LysoSensor Yellow/Blue DND-160, a ratiometric probe whose emission spectrum shifts according to intraluminal pH. CPT1C-KO cells exhibited a significantly lower yellow-to-blue emission ratio than WT cells (Fig. 3D,E), confirming a less acidic lysosomal pH in the absence of CPT1C. We then assessed lysosomal proteolytic activity by measuring cathepsin B activity using the Magic Red cathepsin B assay, a fluorogenic substrate that releases red fluorescence upon cleavage by active cathepsin B. CPT1C-KO cells displayed a significant decrease in Magic Red fluorescence intensity relative to WT cells (Fig. 3F,G), indicating reduced cathepsin B activity and further supporting impaired lysosomal function. Altogether, these results demonstrate that CPT1C is required to maintain proper endolysosomal acidity and lysosomal proteolytic activity in hypothalamic neurons.

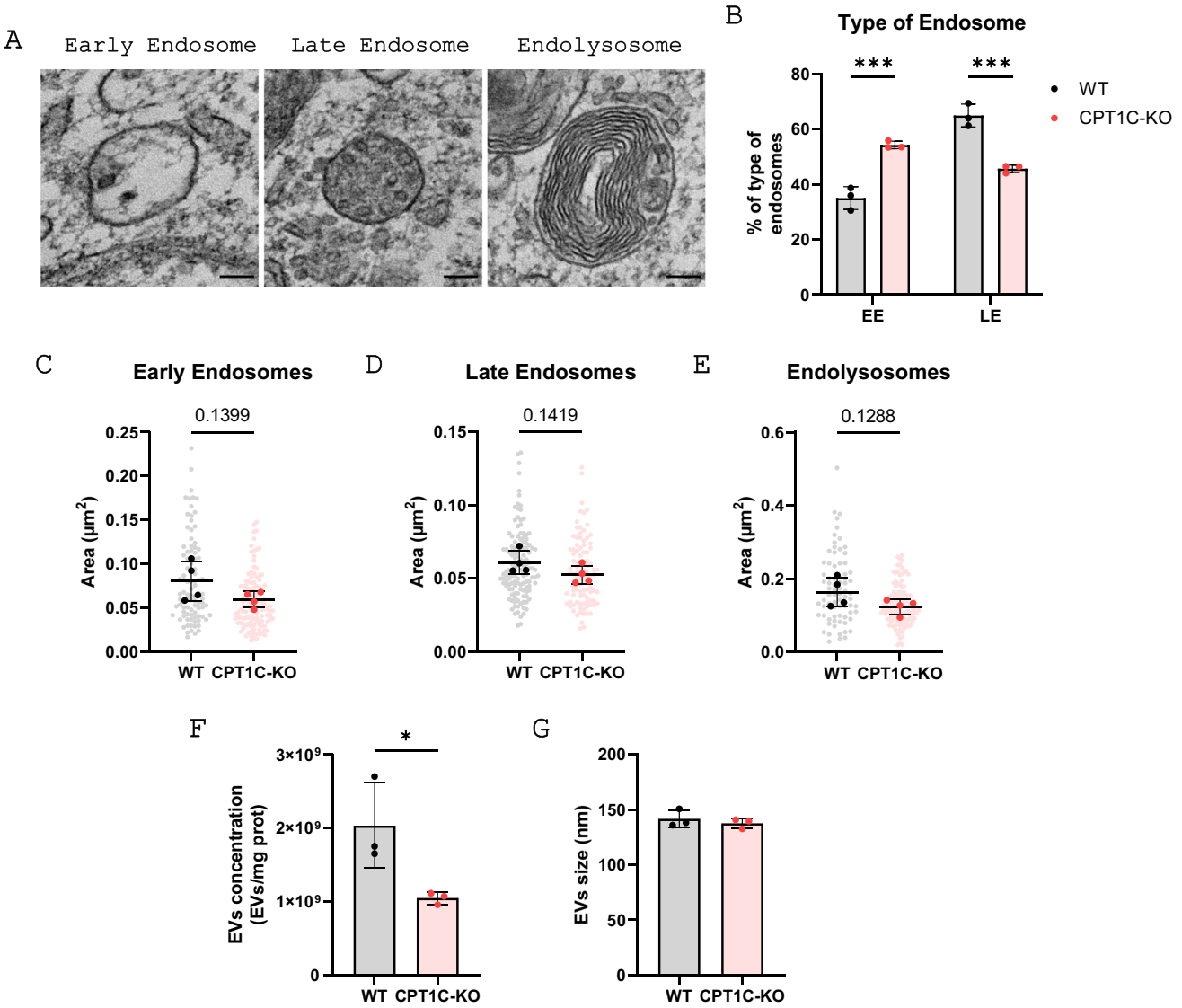


Fig. 2 Endolysosomal ultrastructure in WT and CPT1C KO GT1-7 cells. **A**) Representative electron microscopy images of an early endosome (EE), a late endosome (LE) and an endolysosome. Scale bars = 0.1 µm. **B**) Relative distribution of EE and LE profiles within the total analyzed endosomal population. Percentages were calculated for each genotype and independent experiment. Each dot represents one independent experiment; data are shown as mean ± SD; n = 3 independent experiments. The absolute number of analyzed profiles included in this panel was 63 EE and 112 LE profiles in WT cells, and 103 EE and 88 LE profiles in CPT1C-KO cells. These structures were obtained from 167 WT and 146 CPT1C-KO TEM images. **C**) Area of early endosomes of WT and CPT1C-KO cells (n = 4 independent experiments). Data are shown as mean ± SD. **D**) Area of late endosomes of WT and CPT1C-KO cells (n = 4 independent experiments). Data are shown as mean ± SD. **E**) Area of endolysosomes of WT and CPT1C-KO cells (n = 4 independent experiments). Data are shown as mean ± SD. F-G) Extracellular vesicles (EVs) concentration (**F**) and size (**G**) released from WT and CPT1C-KO cells. The amount of EVs released is normalized per mg protein. (n = 3 independent experiments). Data are shown as mean ± SD

CPT1C-dependent control of ABHD6 activity and BMP homeostasis is nutrient sensitive

We previously showed that the negative regulation of ABHD6 by CPT1C is modulated by the nutritional status of the cell [28]. In addition, hypothalamic CPT1C has been identified as a key mediator of lipid sensing in response to saturated and unsaturated long-chain fatty acids (LCFAs) [34]. Based on these observations, we examined whether CPT1C-dependent regulation of BMP levels is modulated by LCFA overload. To model LCFA overload,

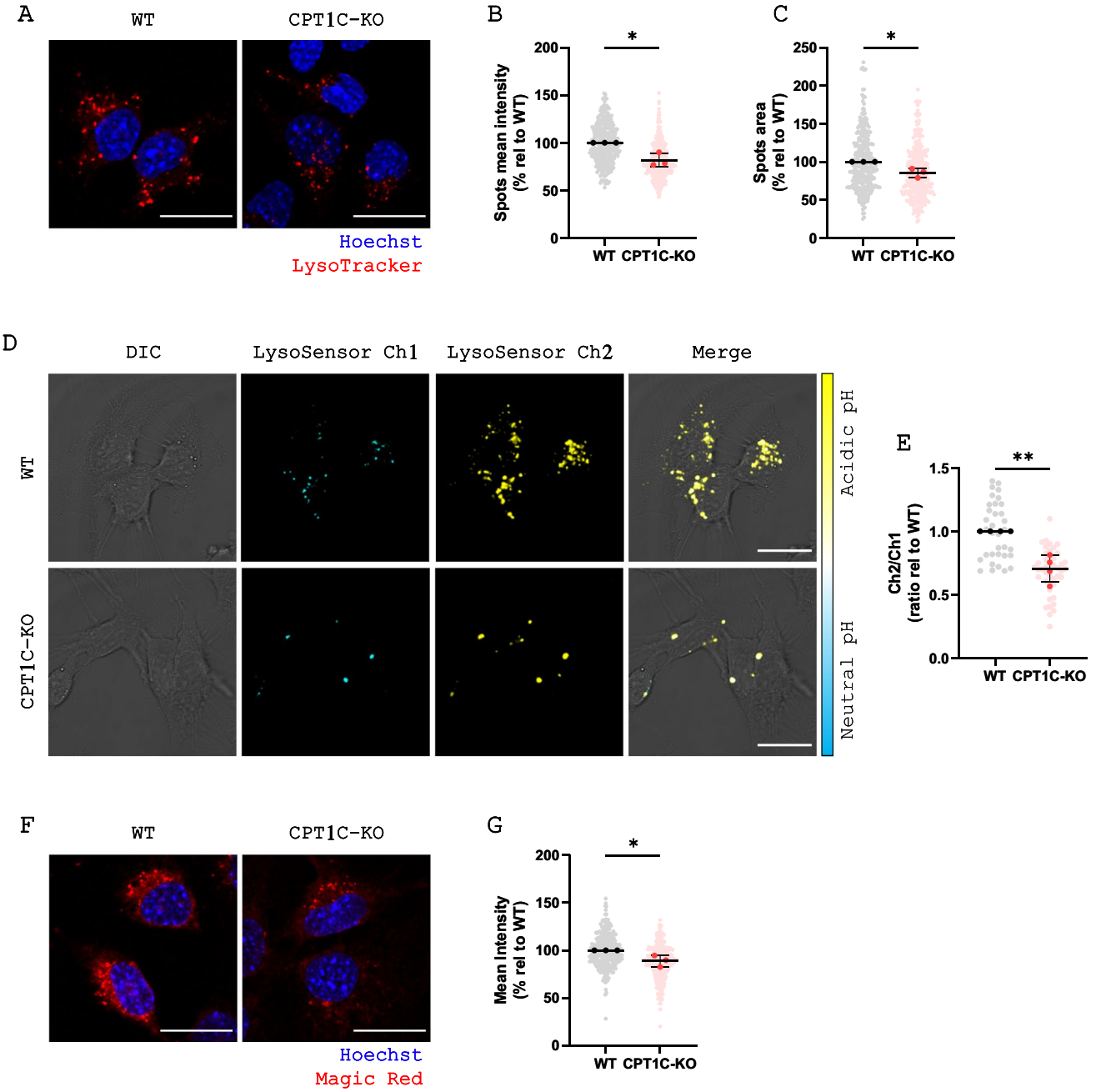


Fig. 3 Lysosomal function in WT and CPT1C KO GT1-7 cells. **A**) Representative confocal images of LysoTracker dye in WT and CPT1C-KO cells. Scale bars = 20 µm. B-C) Quantification of LysoTracker fluorescence intensity (**B**) and dots size (**C**) per cell in WT and CPT1C-KO cells (n = 3 independent experiments). Data are shown as mean ± SD. **D**) Representative confocal images of Magic Red dye in WT and CPT1C-KO cells. Scale bars = 20 µm. **E**) Quantification of Magic Red intensity per cell in WT and CPT1C-KO cells (n = 3 independent experiments). Data are shown as mean ± SD. **F**) Representative confocal images of LysoSensor Yellow/Blue DND-160 dye in WT and CPT1C-KO cells. **G**) Quantification of LysoSensor as the ratio of Ch2/Ch1 per image in WT and CPT1C-KO cells (n = 4 independent experiments). Data are shown as mean ± SD

we selected 300 µM palmitic acid (PA) or oleic acid (OA) based on viability assays showing that 150 and 300 µM LCFA did not significantly reduce GT1-7 cell viability, whereas 500 µM significantly decreased viability (Supplementary Fig. 10). This condition is consistent with previous studies using hypothalamic neuronal models exposed to saturated fatty acids and was used as a control in vitro lipid-overload challenge [41, 42].

WT and CPT1C-KO cells were exposed for 16 h to PA or OA, and BMP levels were quantified by immunocytochemistry. In WT cells, both PA and OA significantly reduced BMP levels relative to BSA-treated controls (Fig. 4A,B). By contrast, BMP levels in CPT1C-KO cells were already low under basal conditions and did not decrease further after LCFA exposure.

These changes were mirrored by ABHD6 activity. Both PA and OA increased ABHD6 hydrolase activity in WT cells, whereas CPT1C-KO cells displayed constitutively elevated ABHD6 activity that was not further enhanced by lipid treatment (Fig. 4C,D). Neither CPT1C nor ABHD6 protein levels changed in response to PA or OA in either genotype (Fig. 4E-G), indicating that lipid-dependent regulation occurs at the level of ABHD6 activity rather than protein abundance. These findings support the idea that CPT1C provides dynamic nutrient-sensitive restraint on ABHD6, thereby preserving BMP homeostasis under basal conditions and enabling adaptation to lipid overload.

CPT1C-dependent regulation of BMP metabolism is conserved in mice and is specifically dysregulated in the hypothalamus upon high-fat diet exposure

To further validate the regulatory role of CPT1C on BMP metabolism in a physiologically relevant context and to determine whether this regulation is altered during nutrient overload in vivo, we measured BMP levels, BMP species distribution, and ABHD6 activity in hypothalamus, hippocampus, and liver from WT and CPT1C-KO mice exposed to short-term HFD feeding. In the hypothalamus, HFD induced a marked reduction in total BMP levels in WT mice, whereas CPT1C-KO mice showed no diet-induced changes and maintained constitutively low BMP levels under both standard diet (SD) and HFD (Fig. 5A), aligning with the results observed in hypothalamic neurons. The reduction in total hypothalamic BMP was driven mainly by decreases in the most abundant polyunsaturated species, particularly a trend in arachidonoyl (40:8)- and in DHA (44:12)-containing BMP species (Fig. 5B).

Consistent with these findings, ABHD6 activity was elevated in the hypothalamus of CPT1C-KO mice under SD, and HFD increased ABHD6 activity selectively in WT mice (Fig. 5C,D). CPT1C and ABHD6 protein levels were unchanged across conditions (Supplementary Fig. 11A-C), indicating that HFD regulates hypothalamic BMP homeostasis through CPT1C-dependent modulation of ABHD6 activity rather than altered protein expression.

To assess whether this regulatory mechanism extends to other brain regions expressing CPT1C, we also examined the hippocampus. In contrast to the hypothalamus, hippocampal total BMP levels remained unchanged across diets and genotypes (Fig. 5E), and only minor variations were detected in the most abundant hippocampal BMP species (Fig. 5F). ABHD6 activity was higher in CPT1C-KO hippocampus than in WT under both SD and HFD, but HFD did not alter ABHD6 activity within either genotype (Fig. 5G,H), and CPT1C and ABHD6 protein levels were again unchanged (Supplementary Fig. 11D-F). Thus, CPT1C modulates basal hippocampal ABHD6 activity, but short-term HFD does not substantially remodel hippocampal BMP homeostasis.

In the liver, where CPT1C is not expressed and ABHD6 regulation of BMP has been demonstrated [11], the response differed from that observed in brain tissue. HFD reduced total hepatic BMP levels in both WT and CPT1C-KO mice (Supplementary Fig. 12A,B), indicating that diet-induced hepatic BMP remodeling occurs independently of CPT1C. Although ABHD6 activity differed between genotypes and diets (Supplementary Fig. 12C,D), these changes did not parallel BMP abundance, consistent with the existence of CPT1C-independent mechanisms regulating hepatic BMP homeostasis.

Together, these in vivo findings establish that CPT1C-dependent control of BMP homeostasis is particularly evident in the hypothalamus, where its metabolism is enhanced by a short-term dietary lipid overload.

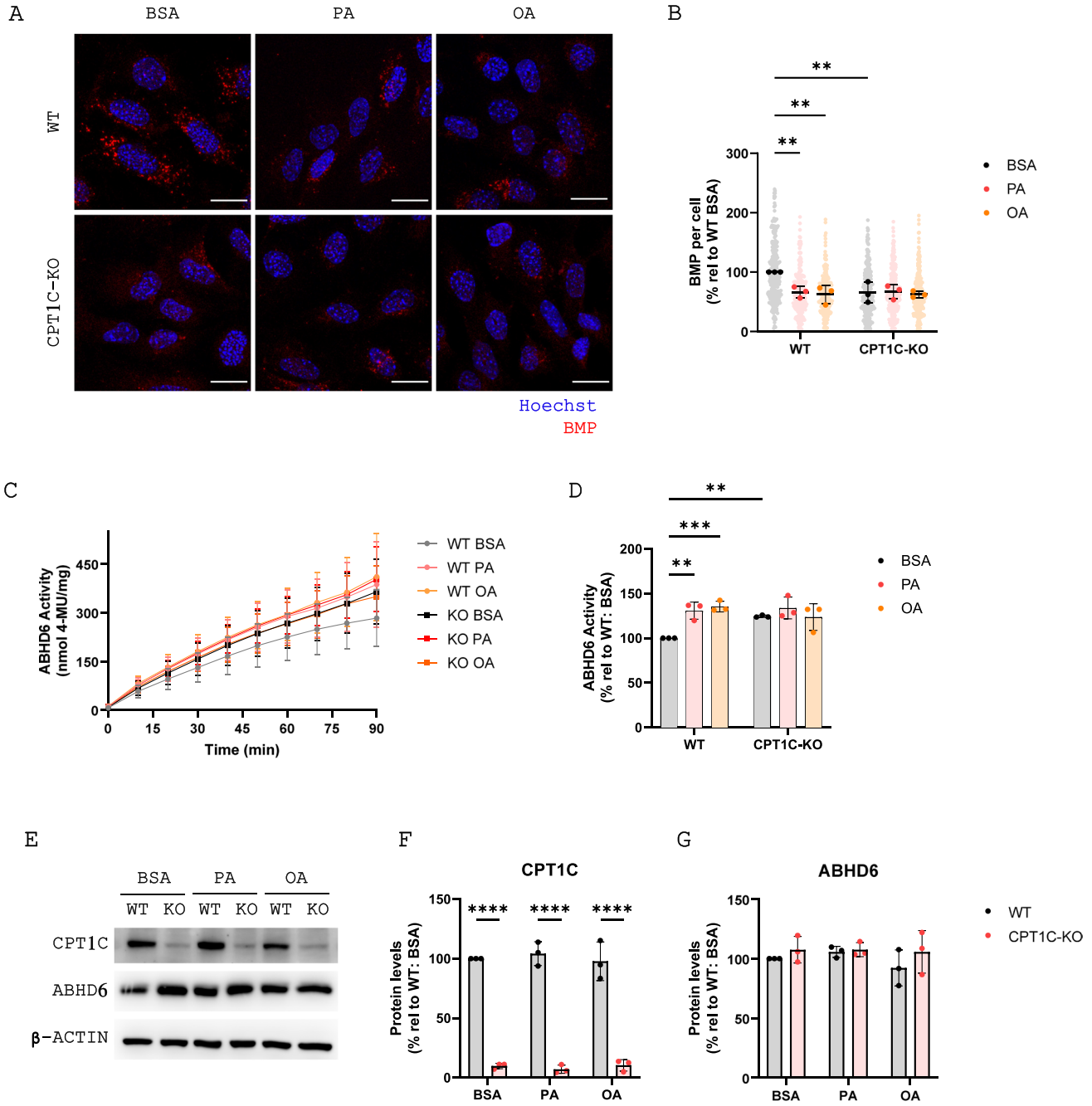


Fig. 4 Fatty acids increase ABHD6 activity and decrease BPM in a way dependent on CPT1C. **A**) Representative confocal images of BMP immunocytochemistry in WT and CPT1C-KO cells after treatment with BSA, 300 µM PA or 300 µM OA for 16 h. **B**) Quantification of BMP intensity per cell of WT and CPT1C-KO cells treated with BSA, PA or OA (n = 3 independent experiments). Data are shown as mean ± SD. C-D) Kinetics (**C**) and quantification (**D**) of ABHD6 activity in WT and CPT1C-KO cells after treatment with BSA, PA or OA. Quantification of hydrolase activity was calculated from the AUCs of graphs shown in (C) (n = 3 independent experiments). Data are shown as mean ± SD. E) Representative image from immunoblotting of CP1C, ABHD6 and β-actin in WT and CPT1C-KO cells treated with BSA, PA or OA. F-G) Immunoblot quantification of CPT1C and ABHD6 (n = 3 independent experiments). Data are shown as mean ± SD

https://doi.org/10.1007/s00018-026-06451-3

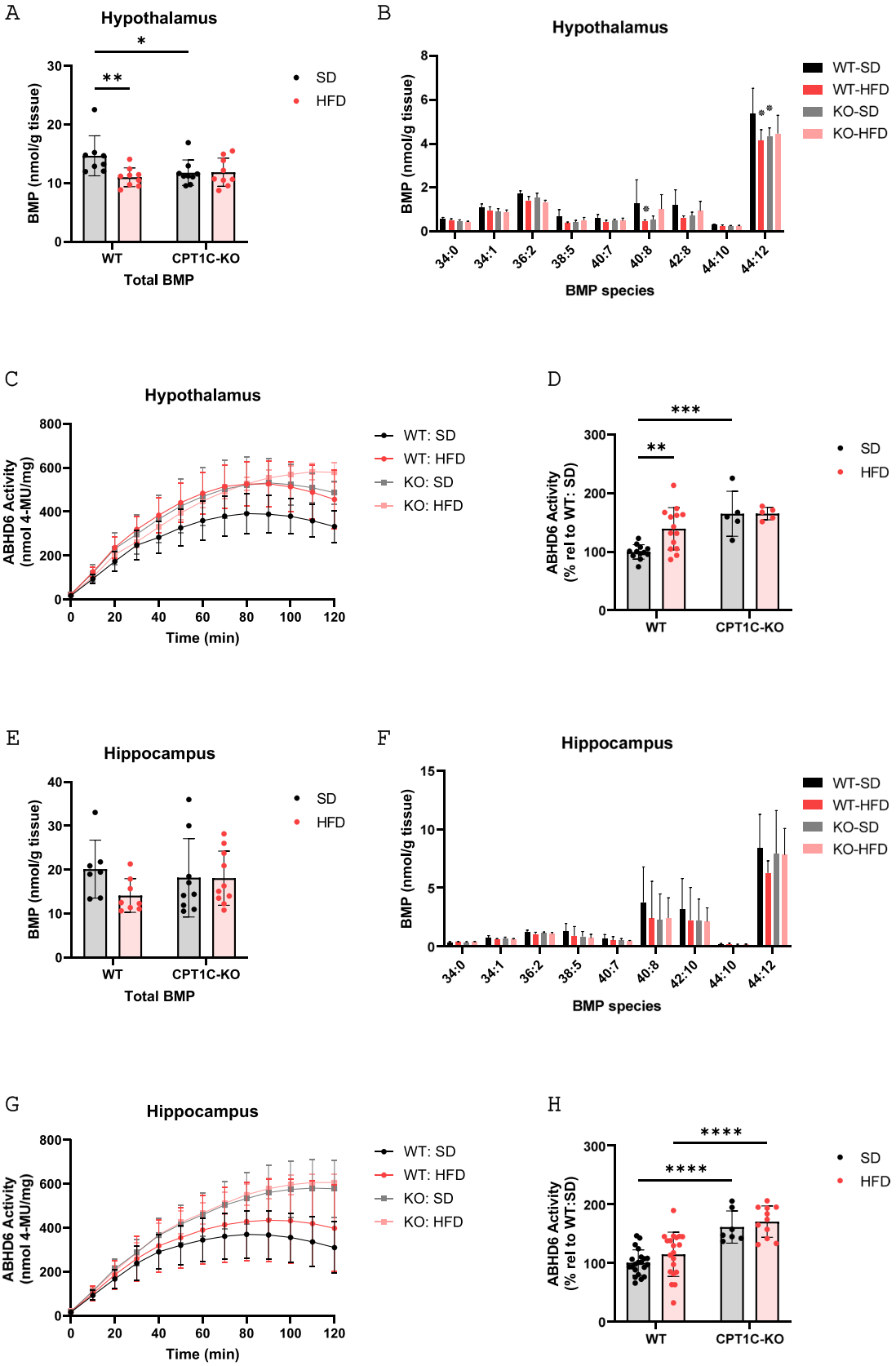


Fig. 5 Effects of short-term HFD on hypothalamic and hippocampal BMP levels and ABHD6 activity in WT and CPT1C-KO mice. A-B) Total hypothalamic BMP content of WT and CPT1C-KO mice fed a SD or HFD for 7 days (**A**) and respective BMP subspecies (**B**) (n≥8 animals). C-D) Kinetics (**C**) and respective quantification (**D**) of hypothalamic ABHD6 activity in WT and CPT1C-KO mice after short-term HFD. Quantification of hydrolase activity was calculated from the AUCs of graphs shown in (C) (n≥5 animals). E–F) Total hippocampal BMP content of WT and CPT1C-KO mice fed a SD or HFD for 7 days (**E**) and respective BMP subspecies (**F**) (n≥8 animals). G-H) Kinetics (**G**) and respective quantification (**H**) of hippocampal ABHD6 activity in WT and CPT1C-KO mice after short-term HFD. Quantification of hydrolase activity was calculated from the AUCs of graphs shown in (C) (n≥5 animals). Data are shown as mean ± SD

Discussion

This study identifies CPT1C as a nutrient-sensitive regulator of BMP homeostasis and endolysosomal function in hypothalamic neurons. Building on our previous finding that CPT1C interacts with ABHD6, and that CPT1C functionally restrains ABHD6 activity [28], we now show that loss of CPT1C increases ABHD6 activity without changing ABHD6 expression, lowers intracellular BMP levels, and is accompanied by defects in endosomal maturation, small EV release, lysosomal acidification, and lysosomal proteolytic activity. Importantly, the same regulatory logic is recapitulated in vivo in the hypothalamus, where short-term HFD increases ABHD6 activity and reduces BMP levels in WT but not CPT1C-deficient mice. Together, these findings place the CPT1C-ABHD6 axis at the interface between nutrient sensing and neuronal BMP homeostasis with effects on the endolysosomal system.

A major conceptual advance of this investigation is the definition of CPT1C as an upstream regulator of ABHD6-dependent control of BMP. Several observations strongly support this conclusion. First, CPT1C deficiency increases ABHD6 activity in hypothalamic neurons and hypothalamic tissue without affecting ABHD6 protein abundance, indicating a regulatory effect at the level of enzymatic activity rather than expression. Second, acute pharmacological inhibition of ABHD6 restores BMP levels in CPT1C-KO cells, indicating that BMP depletion is primarily driven by enhanced hydrolysis. Third, PG supplementation increases BMP in both WT and CPT1C-deficient cells, arguing against a major defect in BMP synthetic capacity. Taken together, these findings support a model in which CPT1C preserves BMP homeostasis by regulating ABHD6 activity.

This model is consistent with the growing but still incomplete understanding of BMP metabolism. ABHD6 has emerged as a major BMP hydrolase in brain and liver [21], but recent studies indicate that BMP homeostasis is governed by multiple enzymes and pathways. In particular, lysosomal phospholipase A2/PLA2G15 has recently been identified as an additional BMP hydrolase, highlighting the existence of spatially distinct routes of BMP catabolism [14]. Likewise, recent work defining enzymes involved in BMP biosynthesis has begun to clarify how BMP pools are generated and maintained [43]. Within this broader framework, our results place the CPT1C-ABHD6 as a nutrient-sensitive regulatory layer that modulates neuronal BMP abundance under changing metabolic conditions, rather than the sole determinant of BMP homeostasis. This positioning is important, because it highlights how metabolic cues can be translated into dynamic remodeling of the endolysosomal lipid environment.

An unresolved mechanistic question concerns how ABHD6 accesses BMP. ABHD6 is positioned on the cytosolic face of membranes [44], whereas BMP is highly enriched in the luminal leaflet of ILVs within late endosomes [6, 45]. A coherent mechanistic framework is provided by the concept of ILV back-fusion, through which ILV membranes can fuse with the endosomal limiting membrane, thereby rendering luminal lipids accessible to cytosol-facing proteins. This process has been proposed for the recycling of cargoes such as mannose-6-phosphate receptor and EGFR, and it is fully compatible with the original proposal that ABHD6 hydrolyzes BMP after its exposure on the limiting membrane [6, 21]. Within this framework, our data identify CPT1C as the upstream factor that determines how strongly this ABHD6-dependent route impacts neuronal BMP homeostasis.

The colocalization analyses provide a spatial support for this model. CPT1C and ABHD6 showed localization compatible with the ER compartment and partial overlap with each other, in agreement with our previous demonstration of a CPT1C-ABHD6 interaction [28]. In addition, both proteins showed partial colocalization with

LAMP1-positive and BMP-positive structures, supporting the possibility that CPT1C-dependent regulation of ABHD6 occurs in proximity to LE/lysosomal BMP-containing compartments. Given the predominant ER localization of CPT1C and the enrichment of BMP in LEs, these observations are consistent with a model in which CPT1C regulates ABHD6 at ER-endolysosomal interfaces or membrane contact sites. However, these colocalization data should be interpreted as evidence of spatial compatibility rather than definitive proof of contact-site-dependent regulation.

The downstream endolysosomal phenotypes observed in CPT1C-deficient neurons provide a functional link between BMP depletion and impaired endolysosomal maturation. BMP is required for the organization of ILVs, late endosome maturation, cholesterol handling, and lysosomal degradative capacity [9]. Accordingly, the increased proportion of EE profiles, together with the reduced proportion and smaller size of LE profiles observed in CPT1C-KO cells, is consistent with impaired progression toward mature ILV-rich late endosomal compartments, reflecting altered endosomal maturation dynamics within the endolysosomal pathway.

This interpretation is supported by the downstream functional alterations observed in CPT1C-KO cells. A reduction or remodeling of mature ILV-containing LE would be expected to affect both small EV biogenesis and lysosomal delivery, since multivesicular LEs can either fuse with the plasma membrane to release exosomes or mature/fuse with lysosomes to support cargo degradation [6]. In line with this, CPT1C-KO cells showed reduced small EV release, impaired lysosomal acidification, and decreased cathepsin activity. These findings align with recent work showing that decreased BMP compromises endosomal membrane organization and lysosomal competence [45], as well as studies showing that BMP-deficient lysosomes lose ILVs and develop marked defects in lipid degradation and cholesterol handling [13, 45]. Thus, the endosomal population shift is not an isolated morphological observation, but part of a broader endolysosomal phenotype in which ABHD6 hyperactivation reduces BMP availability, disrupts late endosomal membrane organization, and compromises downstream endolysosomal function.

The reduction in cholesterol observed in CPT1C-deficient neurons further supports the link between BMP homeostasis and endolysosomal lipid organization. BMP has been proposed to promote both the structural capacity of endosomes to accommodate cholesterol through ILV formation and the export of cholesterol from endolysosomal compartments by interactions with cholesterol transport machinery such as NPC2 [35, 36, 46]. In our system, CPT1C-KO cells displayed reduced filipin staining, indicating lower levels and/or altered distribution of filipin-detectable free cholesterol. Importantly, this imaging-based observation was corroborated by an Amplex Red-based enzymatic assay after lipid extraction, which showed reduced total cellular cholesterol content in CPT1C-KO cells. Thus, these findings indicate that CPT1C deficiency is associated with an alteration in cellular cholesterol homeostasis. The close parallel between reduced BMP levels, lower ILV density, decreased filipin staining and total cholesterol content, is therefore aligned with impaired BMP-dependent cholesterol organization within the endolysosomal pathway. This is particularly relevant in neurons, where tight control of membrane lipid composition is essential for organelle identity, trafficking, and proteostatic resilience [47, 48]. Importantly, this phenotype should not be interpreted as a simple NPC-like lysosomal cholesterol-trapping defect. In contrast to NPC disease models, BMP levels are reduced but not abolished in CPT1C-deficient neurons, and the NPC1/NPC2 cholesterol export machinery is not genetically disrupted. Therefore, CPT1C deficiency may alter cholesterol abundance and organization within the endolysosomal system without necessarily producing massive lysosomal cholesterol accumulation.

The effects of CPT1C deficiency on EV release provide an additional functional link between BMP homeostasis and neuronal membrane trafficking. ILVs within late endosomes can either be delivered to lysosomes for degradation or released as exosomes following fusion with the plasma membrane [6]. The reduced small EV output in CPT1C-KO cells, together with their shift toward a less mature endosomal population, supports the notion that disruption of the CPT1C-ABHD6-BMP axis impairs not only degradative flux but also endosomal export and intercellular communication. This is likely to be particularly relevant in neurons, where EVs contribute to synaptic plasticity, metabolic support, inflammatory signalling, and maintenance of endosomal pathway integrity [49, 50]. Of particular interest, BMP-containing exosomes have been proposed to function as a homeostatic route

to relieve lysosomal stress [51], and recent work in hypothalamic neurons has suggested that neuronal EVs can modulate energy balance and that this signalling is altered by palmitate exposure [52]. Thus, the reduction in small EV release observed here suggests that the CPT1C-ABHD6-BMP axis may influence hypothalamic physiology through a dual effect on intracellular endolysosomal competence and EV-mediated neuronal communication.

The lysosomal phenotype of CPT1C-deficient neurons is also coherent with defective BMP homeostasis. Together with the reduced proportion of ILV-rich LE profiles, CPT1C-KO cells show smaller LysoTracker-positive compartments, reduced LysoTracker intensity, lower LysoSensor Yellow/Blue ratio, and decreased cathepsin B activity. Because additional quantification showed no significant differences in LysoTracker-positive puncta number or distance to the nucleus, these findings are more consistent with impaired organization and acidification of acidic endolysosomal compartments than with reduced compartment abundance or gross intracellular redistribution. The size and acidification state of lysosomes are tightly linked to degradative performance and cellular homeostasis [53, 54]. In this regard, it is notable that increasing BMP through PG supplementation has been reported to re-acidify lysosomes and improve lysosomal homeostasis in NPC1 fibroblasts [8], further supporting the idea that the reduced lysosomal competence observed here is a direct functional consequence of altered BMP homeostasis. More broadly, these findings place CPT1C within the molecular framework that sustains the progressive maturation of endosomes into fully functional degradative organelles. BMP depletion should not be interpreted as the only lipid alteration caused by CPT1C deficiency. Given that ABHD6 also hydrolyzes monoacylglycerols, including 2-AG, and that CPT1C-ABHD6 regulation has previously been linked to 2-AG signaling, future targeted lipidomic studies will be required to define the broader impact of CPT1C loss on MAGs, phosphoinositides and other endomembrane lipids.

One of the most important features of the pathway described here is its nutrient sensitivity. In WT hypothalamic neurons, lipid overload induced by either palmitate or oleate increases ABHD6 activity and lowers BMP levels, whereas CPT1C-deficient neurons display constitutively elevated ABHD6 activity and low BMP levels that fail to further adapt to lipid excess. A similar pattern is observed in the hypothalamus of HFD-fed mice. These findings indicate that CPT1C does not simply act as a static inhibitor of ABHD6. Rather, CPT1C provides dynamic inhibitory control over ABHD6 that is modulated by metabolic state, thereby preserving a homeostatic BMP pool under basal conditions while allowing adaptive remodeling under nutrient challenge. This interpretation fits with previous evidence that CPT1C senses metabolic cues, including changes in malonyl-CoA, and couples them to ABHD6 regulation [28, 31, 55]. It is well established that fatty acids inhibit malonyl-CoA synthesis [55], and we have previously shown that under these conditions CPT1C fails to fully inhibit ABHD6 [28]. In particular, a malonyl-CoA-insensitive CPT1C mutant failed to support the normal nutrient-dependent regulation of ABHD6, indicating that the malonyl-CoA-sensing capacity of CPT1C is required for this coupling [28]. This could explain the increase in ABHD6 activity and the enhanced BMP degradation observed. In this context of lipid overload, the phenotype of CPT1C deficiency is not only one of chronically reduced BMP abundance, but also one of impaired adaptive plasticity in endolysosomal lipid homeostasis. Thus, the data supports a working model in which lipid availability modulates CPT1C-dependent control of ABHD6 activity, thereby affecting BMP abundance and downstream endosomal maturation, lysosomal acidification and proteolytic competence. However, this sequence should be interpreted as a mechanistic model rather than as a directly demonstrated time-resolved cascade.

The regional specificity observed in vivo further strengthens this interpretation. Whereas the hypothalamus showed a clear diet-dependent remodeling of BMP homeostasis, the hippocampus did not exhibit major changes after short-term HFD, despite elevated basal ABHD6 activity in CPT1C-deficient tissue. This regional divergence is fully consistent with the privileged role of the hypothalamus as an early nutrient-sensing brain region, characterized by greater exposure to circulating metabolic cues and a central role in whole-body energy homeostasis [56]. It is also consistent with the known function of CPT1C as a neuronal lipid sensor that responds to metabolic cues such as malonyl-CoA and long-chain fatty acids [29, 55]. Thus, hypothalamic neurons may be particularly sensitive to short-term dietary lipid overload because they combine high nutrient-sensing capacity with CPT1C-dependent regulation of ABHD6 activity. By contrast, the hippocampus may require a more prolonged or severe

metabolic challenge to undergo comparable BMP remodeling. Although CPT1C is expressed in the hippocampus and CPT1C deficiency increased basal ABHD6 activity in this region, short-term HFD did not further modify hippocampal ABHD6 activity or BMP levels. This suggests that hippocampal CPT1C-ABHD6 coupling may regulate basal endolysosomal lipid homeostasis but is less acutely engaged by dietary lipid excess than the hypothalamic pathway. Differences in neuronal populations, local lipid handling, blood–brain barrier exposure, and metabolic sensing programs may all contribute to this region-specific response. This regional dimension is highly relevant, as it links the CPT1C-ABHD6-BMP axis specifically to the neuronal populations that first decode changes in nutrient availability.

The liver exhibited a distinct pattern, as expected from the lack of CPT1C expression in this tissue. HFD reduced hepatic BMP levels in both WT and CPT1C-KO mice, indicating that short-term diet-induced hepatic BMP remodeling occurs independently of CPT1C. Genotype-dependent differences in hepatic BMP and ABHD6 activity in global CPT1C-deficient mice are therefore unlikely to reflect a direct cell-autonomous mechanism. Instead, they may arise from indirect systemic adaptations secondary to neuronal CPT1C deficiency. Notably, previous studies have reported increased hepatic BMP after chronic HFD (12 weeks) [12, 57], in contrast to the reduction observed here after short-term exposure. Although these studies are not directly comparable, the discrepancy raises the possibility that hepatic BMP homeostasis changes dynamically during the progression from early nutrient excess to established obesity.

The tissue-specific remodeling of BMP species observed here further supports the notion that BMP homeostasis is highly context dependent. In hypothalamus and hippocampus, the predominant species were enriched in polyunsaturated fatty acids, particularly DHA, and the most prominent diet-dependent changes involved arachidonoyl- and DHA-containing BMP species. In liver, by contrast, HFD preferentially altered oleate-, linoleate-, and DHA-containing species. This tissue-specific remodeling is consistent with prior work showing that BMP fatty-acyl composition differs markedly across tissues and can change in disease-specific ways [11, 12]. These compositional differences probably reflect tissue-specific control of BMP synthesis, remodeling, and degradation, as well as differences in local lipid availability and lipid-sensing mechanisms, and may ultimately help explain why BMP functions and disease associations vary across organs. In this regard, the hypothalamic enrichment in highly unsaturated BMP species may be especially relevant for neuronal membrane dynamics and metabolic responsiveness.

Overall, our findings identify CPT1C as a previously unrecognized regulator of neuronal BMP homeostasis. By restraining ABHD6 activity in a nutrient-sensitive manner, CPT1C preserves a BMP pool that is required for efficient endosomal maturation, cholesterol handling, small EV release, and lysosomal function (Fig. 6). These results establish a mechanistic link between neuronal metabolic sensing and endolysosomal lipid homeostasis and position the hypothalamus as a particularly sensitive site in which this coupling becomes functionally relevant under lipid overload. In this way, the CPT1C-ABHD6-BMP axis emerges as a mechanism through which metabolic stress can be translated into endolysosomal dysfunction in hypothalamic neurons, with clear implications for obesity-associated hypothalamic dysfunction and, more broadly, for disorders in which lysosomal lipid homeostasis is compromised. However, the specific impact of this pathway across other neuronal populations, and its potential contribution to human metabolic disease remain to be established.

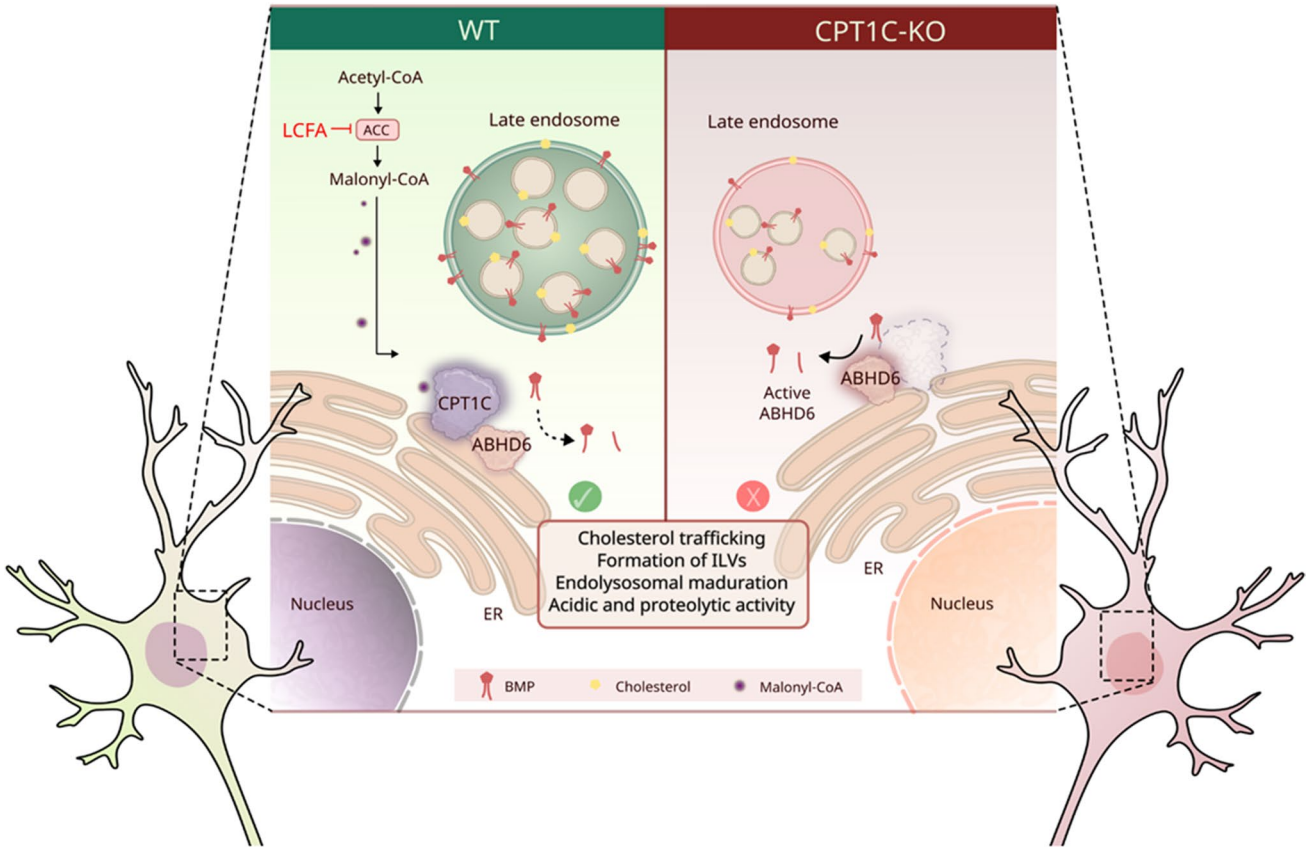


Fig. 6 Model of CPT1C-dependent regulation of BMP homeostasis in hypothalamic neurons. CPT1C restrains ABHD6 activity to preserve BMP levels and sustain endolysosomal maturation and function in WT hypothalamic neurons. Loss of CPT1C enhances ABHD6-dependent BMP hydrolysis, reduces BMP abundance, and impairs ILV formation, cholesterol trafficking, lysosomal acidification, proteolytic activity, and EV release, leading to a more immature endolysosomal compartment

Supplementary Information The online version contains supplementary material available at https://doi.org/10.1007/s00018-026-06451-3.

Acknowledgements This study was supported by the Spanish Ministry of Science and Innovation (MCIN) (PID2020-114953RB-C22 and PID2023-146716OB-I00 to NC and RRR) co-funded by the European Regional Development Fund, the Centro de Investigación Biomédica en Red-Fisiopatología de la Obesidad y Nutrición (CIBEROBN). The measurement of exosomes has been performed by the ICTS "NANBIOSIS", more specifically by Unit 6. Unit of the CIBER in Bioengineering, Biomaterials & Nanomedicine (CIBER-BBN) at the Barcelona Materials Science Institute.

Author contributions A.C. Reguera: Methodology, Investigation, Data curation, Writing-original draft. C. Miralpeix: Methodology, Investigation, Writing-review & editing. M. Bernard: Methodology, Data curation. S. Zagmutt: Methodology, Data curation. M. Bolaños-Hurtado: Methodology, Data curation. C. Palacín: Methodology, Data curation. A. Fuentes: Methodology, Data curation. M. Rodriguez-Garcia: Methodology, Data curation. A. Fosch: Methodology, Data curation. J. Garcia-Chica: Methodology, Data curation. R. Barnadas-Rodriguez: Methodology, Data curation, Writing-review & editing. N. Fawzy: Methodology, Data curation, Writing-review & editing. R. Zimmermann: Writing-review & editing, Resources, Methodology. E. Eden: Writing-review & editing, Resources, Supervision, Methodology. N. Casals: Writing-review & editing, Supervision, Funding acquisition, Conceptualization, Resources. R. Rodriguez-Rodriguez: Writing-original draft, Supervision, Funding acquisition, Conceptualization, Project administration.

Data availability The authors confirm that the data supporting the findings of this study are available within the article and its Supplementary Information. Additional data supporting the findings of this study are available from the corresponding author upon reasonable request.

Declarations

Competing interests The authors declare no competing interests.

Open Access This article is licensed under a Creative Commons Attribution-NonCommercial-NoDerivatives 4.0 International License, which permits any non-commercial use, sharing, distribution and reproduction in any medium or format, as long as you give appropriate credit to the original author(s) and the source, provide a link to the Creative Commons licence, and indicate if you modified the licensed material. You do not have permission under this licence to share adapted material derived from this article or parts of it. The images or other third party material in this article are included in the article's Creative Commons licence, unless indicated otherwise in a credit line to the material. If material is not included in the article's Creative Commons licence and your intended use is not permitted by statutory regulation or exceeds the permitted use, you will need to obtain permission directly from the copyright holder. To view a copy of this licence, visit http://creativecommons.org/licenses/by-nc-nd/4.0/.

References

1. De Tito S, Tooze SA (2026) Lysosomal homeostasis at the crossroads of neurodegeneration. J Clin Investig 136. https://doi.org/10.1172/JCI199845
2. Udayar V, Chen Y, Sidransky E, Jagasia R (2022) Lysosomal dysfunction in neurodegeneration: emerging concepts and methods. Trends Neurosci 45:184–199. https://doi.org/10.1016/j.tins.2021.12.004
3. Settembre C, Perera RM (2024) Lysosomes as coordinators of cellular catabolism, metabolic signalling and organ physiology. Nat Rev Mol Cell Biol 25:223–245. https://doi.org/10.1038/s41580-023-00676-x
4. Radulovic M, Yang C, Stenmark H (2026) Lysosomal membrane homeostasis and its importance in physiology and disease. Nat Rev Mol Cell Biol 27:71–87. https://doi.org/10.1038/s41580-025-00873-w
5. Gilleron J, Gerdes JM, Zeigerer A (2019) Metabolic regulation through the endosomal system. Traffic 20:552–570. https://doi.org/10.1111/tra.12670
6. Gruenberg J (2020) Life in the lumen: the multivesicular endosome. Traffic 21:76–93. https://doi.org/10.1111/tra.12715
7. Feng B, Beaven AH, Hossein A, Sodt AJ (2024) Unveiling the mechanics of lysobisphosphatidic acid in late-endosome/lysosome cholesterol trafficking. Biophys J 123:370a. https://doi.org/10.1016/j.bpj.2023.11.2258
8. Ilnytska O, Jeziorek M, Lai K et al (2021) Lysobisphosphatidic acid (LBPA) enrichment promotes cholesterol egress via exosomes in Niemann Pick type C1 deficient cells Biochimica et Biophysica Acta (BBA). Mol Cell Biol Lipids 1866:158916. https://doi.org/10.1016/j.bbalip.2021.158916
9. Showalter MR, Berg AL, Nagourney A et al (2020) The emerging and diverse roles of Bis(monoacylglycero) phosphate lipids in cellular physiology and disease. Int J Mol Sci 21:8067. https://doi.org/10.3390/ijms21218067
10. Medoh UN, Abu-Remaileh M (2024) The Bis(monoacylglycero)-phosphate hypothesis: from lysosomal function to therapeutic avenues. Annu Rev Biochem 93:447–469. https://doi.org/10.1146/annurev-biochem-092823-113814
11. Grabner GF, Fawzy N, Schreiber R, et al (2020) Metabolic regulation of the lysosomal cofactor bis(monoacylglycero) phosphate in mice. J Lipid Res 995–1003. https://doi.org/10.1194/jlr.ra119000516
12. Grabner GF, Fawzy N, Pribasnig MA et al (2019) Metabolic disease and ABHD6 alter the circulating bis(monoacylglycerol) phosphate profile in mice and humans. J Lipid Res 60:1020–1031. https://doi.org/10.1194/jlr.M093351
13. Singh S, Dransfeld UE, Ambaw YA et al (2024) PLD3 and PLD4 synthesize S,S-BMP, a key phospholipid enabling lipid degradation in lysosomes. Cell 187:6820-6834.e24. https://doi.org/10.1016/j.cell.2024.09.036
14. Nyame K, Xiong J, Alsohybe HN et al (2025) PLA2G15 is a BMP hydrolase and its targeting ameliorates lysosomal disease. Nature 642:474–483. https://doi.org/10.1038/s41586-025-08942-y
15. Miranda AM, Lasiecka ZM, Xu Y et al (2018) Neuronal lysosomal dysfunction releases exosomes harboring APP C-terminal fragments and unique lipid signatures. Nat Commun 9:291. https://doi.org/10.1038/s41467-017-02533-w
16. Moreau D, Vacca F, Vossio S, et al (2019) Drug-induced increase in lysobisphosphatidic acid reduces the cholesterol overload in Niemann–Pick type C cells and mice. EMBO Rep 20. https://doi.org/10.15252/embr.201847055
17. Canfrán-Duque A, Barrio L, Lerma M et al (2016) First-generation antipsychotic haloperidol alters the functionality of the late endosomal/lysosomal compartment in vitro. Int J Mol Sci 17:404. https://doi.org/10.3390/ijms17030404
18. Ebner M, Puchkov D, López-Ortega O et al (2023) Nutrient-regulated control of lysosome function by signaling lipid conversion. Cell 186:5328-5346.e26. https://doi.org/10.1016/j.cell.2023.09.027
19. Hernández-Cáceres MP, Cereceda K, Hernández S, et al (2020) Palmitic acid reduces the autophagic flux in hypothalamic neurons by impairing autophagosome-lysosome fusion and endolysosomal dynamics. Mol Cell Oncol 7. https://doi.org/10.1080/23723556.2020.1789418
20. Cheong LYT, Saipuljumri EN, Loi GWZ et al (2025) Autolysosomal dysfunction in obesity-induced metabolic inflammation and related disorders. Curr Obes Rep 14:43. https://doi.org/10.1007/s13679-025-00638-8

21. Pribasnig MA, Mrak I, Grabner GF et al (2015) α/β hydrolase domain-containing 6 (ABHD6) degrades the late endosomal/lysosomal lipid bis(monoacylglycero)phosphate. J Biol Chem 290:29869–29881. https://doi.org/10.1074/jbc.M115.669168
22. Cao JK, Kaplan J, Stella N (2019) ABHD6: its place in endocannabinoid signaling and beyond. Trends Pharmacol Sci 40:267–277. https://doi.org/10.1016/j.tips.2019.02.002
23. Thomas G, Betters JL, Lord CC et al (2013) The serine hydrolase ABHD6 is a critical regulator of the metabolic syndrome. Cell Rep 5:508–520. https://doi.org/10.1016/j.celrep.2013.08.047
24. Miralpeix C, Reguera AC, Fosch A et al (2021) Hypothalamic endocannabinoids in obesity: an old story with new challenges. Cell Mol Life Sci 78:7469–7490. https://doi.org/10.1007/s00018-021-04002-6
25. Falguières T, Luyet P-P, Gruenberg J (2009) Molecular assemblies and membrane domains in multivesicular endosome dynamics. Exp Cell Res 315:1567–1573. https://doi.org/10.1016/j.yexcr.2008.12.006
26. Fisette A, Tobin S, Décarie-Spain L et al (2016) α/β-Hydrolase domain 6 in the ventromedial hypothalamus controls energy metabolism flexibility. Cell Rep 17:1217–1226. https://doi.org/10.1016/j.celrep.2016.10.004
27. Poursharifi P, Madiraju SRM, Prentki M (2017) Monoacylglycerol signalling and ABHD6 in health and disease. Diabetes Obes Metab 19:76–89. https://doi.org/10.1111/dom.13008
28. Miralpeix C, Reguera AC, Fosch A et al (2021) Carnitine palmitoyltransferase 1C negatively regulates the endocannabinoid hydrolase ABHD6 in mice, depending on nutritional status. Br J Pharmacol 178:1507–1523. https://doi.org/10.1111/bph.15377
29. Rodríguez-Rodríguez R, Fosch A, Garcia-Chica J et al (2023) Targeting carnitine palmitoyltransferase 1 isoforms in the hypothalamus: A promising strategy to regulate energy balance. J Neuroendocrinol 35:e13234
30. Rodríguez-Rodríguez R, Baena M, Zagmutt S et al (2025) International Union of Basic and Clinical Pharmacology: Fundamental insights and clinical relevance regarding the carnitine palmitoyltransferase family of enzymes. Pharmacol Rev 77:100051. https://doi.org/10.1016/J.PHARMR.2025.100051
31. Casas M, Fadó R, Domínguez JL, et al (2020) Sensing of nutrients by CPT1C controls SAC1 activity to regulate AMPA receptor trafficking. J Cell Biol 219. https://doi.org/10.1083/JCB.201912045
32. Palomo-Guerrero M, Fadó R, Casas M et al (2019) Sensing of nutrients by CPT1C regulates late endosome/lysosome anterograde transport and axon growth. Elife 8:1–26. https://doi.org/10.7554/eLife.51063
33. Ran FA, Hsu PD, Wright J et al (2013) Genome engineering using the CRISPR-Cas9 system. Nat Protoc 8:2281–2308. https://doi.org/10.1038/nprot.2013.143
34. Fosch A, Rodriguez-Garcia M, Miralpeix C et al (2023) Central regulation of brown fat thermogenesis in response to saturated or unsaturated long-chain fatty acids. Int J Mol Sci 24:1697. https://doi.org/10.3390/ijms24021697
35. Chevallier J, Chamoun Z, Jiang G et al (2008) Lysobisphosphatidic acid controls endosomal cholesterol levels. J Biol Chem 283:27871–27880. https://doi.org/10.1074/jbc.M801463200
36. McCauliff LA, Langan A, Li R, et al (2019) Intracellular cholesterol trafficking is dependent upon NPC2 interaction with lysobisphosphatidic acid. Elife 8. https://doi.org/10.7554/eLife.50832
37. Barral DC, Staiano L, Guimas Almeida C et al (2022) Current methods to analyze lysosome morphology, positioning, motility and function. Traffic 23:238–269. https://doi.org/10.1111/tra.12839
38. Solana-Balaguer J, Campoy-Campos G, Martín-Flores N, et al (2023) Neuron-derived extracellular vesicles contain synaptic proteins, promote spine formation, activate TrkB-mediated signalling and preserve neuronal complexity. J Extracell Vesicles 12. https://doi.org/10.1002/jev2.12355
39. Matyash V, Liebisch G, Kurzchalia TV et al (2008) Lipid extraction by methyl-tert-butyl ether for high-throughput lipidomics. J Lipid Res 49:1137–1146. https://doi.org/10.1194/jlr.D700041-JLR200
40. Kobayashi T, Beuchat MH, Lindsay M et al (1999) Late endosomal membranes rich in lysobisphosphatidic acid regulate cholesterol transport. Nat Cell Biol 1:113–118. https://doi.org/10.1038/10084
41. Valencia FP, Marino AF, Noutsos C, Poon K (2022) Concentration-dependent change in hypothalamic neuronal transcriptome by the dietary fatty acids: oleic and palmitic acids. J Nutr Biochem 106:109033. https://doi.org/10.1016/j.jnutbio.2022.109033
42. Choi SJ, Kim F, Schwartz MW, Wisse BE (2010) Cultured hypothalamic neurons are resistant to inflammation and insulin resistance induced by saturated fatty acids. Am J Physiol Endocrinol Metab 298:E1122–E1130. https://doi.org/10.1152/ajpendo.00006.2010
43. Bulfon D, Breithofer J, Grabner GF et al (2024) Functionally overlapping intra- and extralysosomal pathways promote bis(monoacylglycero)phosphate synthesis in mammalian cells. Nat Commun 15:9937. https://doi.org/10.1038/s41467-024-54213-1
44. Pusch L-M, Riegler-Berket L, Oberer M et al (2022) α/β-Hydrolase domain-containing 6 (ABHD6)— a multifunctional lipid hydrolase. Metabolites 12:761. https://doi.org/10.3390/metabo12080761
45. Medoh U (2025) The missing piece: solving the 50-year puzzle of BMP synthesis in neurodegeneration. Science 390:685–686. https://doi.org/10.1126/science.aec9580

46. Enkavi G, Mikkolainen H, Güngör B et al (2017) Concerted regulation of npc2 binding to endosomal/lysosomal membranes by bis(monoacylglycero)phosphate and sphingomyelin. PLoS Comput Biol 13:e1005831. https://doi.org/10.1371/journal.pcbi.1005831
47. Egawa J, Pearn ML, Lemkuil BP et al (2016) Membrane lipid rafts and neurobiology: age-related changes in membrane lipids and loss of neuronal function. J Physiol 594:4565–4579. https://doi.org/10.1113/JP270590
48. Hanus C, Ehlers MD (2016) Specialization of biosynthetic membrane trafficking for neuronal form and function. Curr Opin Neurobiol 39:8–16. https://doi.org/10.1016/j.conb.2016.03.004
49. Mathews PM, Levy E (2019) Exosome Production Is Key to Neuronal Endosomal Pathway Integrity in Neurodegenerative Diseases. Front Neurosci 13. https://doi.org/10.3389/fnins.2019.01347
50. Huo L, Du X, Li X, et al (2021) The Emerging Role of Neural Cell-Derived Exosomes in Intercellular Communication in Health and Neurodegenerative Diseases. Front Neurosci 15. https://doi.org/10.3389/fnins.2021.738442
51. Miranda AM, Di Paolo G (2018) Endolysosomal dysfunction and exosome secretion: implications for neurodegenerative disorders. Cell Stress 2:115–118. https://doi.org/10.15698/cst2018.05.136
52. McIlwraith EK, Belsham DD (2023) Palmitate alters miRNA content of small extracellular vesicles secreted from NPY/AgRP-expressing hypothalamic neurons. Brain Res 1810:148367. https://doi.org/10.1016/j.brainres.2023.148367
53. de Araujo MEG, Liebscher G, Hess MW, Huber LA (2020) Lysosomal size matters. Traffic 21:60–75. https://doi.org/10.1111/tra.12714
54. Appelqvist H, Wäster P, Kågedal K, Öllinger K (2013) The lysosome: from waste bag to potential therapeutic target. J Mol Cell Biol 5:214–226. https://doi.org/10.1093/jmcb/mjt022
55. Fadó R, Rodríguez-Rodríguez R, Casals N (2021) The return of malonyl-CoA to the brain: cognition and other stories. Prog Lipid Res 81:101071. https://doi.org/10.1016/j.plipres.2020.101071
56. Haddad-Tóvolli R, Dragano NR V., Ramalho AFS, Velloso LA (2017) Development and Function of the Blood-Brain Barrier in the Context of Metabolic Control. Front Neurosci 11. https://doi.org/10.3389/fnins.2017.00224
57. d'Avignon DA, Puchalska P, Ercal B, et al (2018) Hepatic ketogenic insufficiency reprograms hepatic glycogen metabolism and the lipidome. JCI Insight 3. https://doi.org/10.1172/jci.insight.99762

Publisher's Note Springer Nature remains neutral with regard to jurisdictional claims in published maps and institutional affiliations.

Authors and Affiliations

Ana Cristina Reguera[1] · Cristina Miralpeix[1] · Maribel Bernard[1] · Sebastián Zagmutt[1] · Montserrat Bolaños-Hurtado[1] · Carlos Palacín[1] · Andrea Fuentes[1] · María Rodríguez-García[1] · Anna Fosch[1] · Jesús Garcia-Chica[1] · Ramon Barnadas-Rodríguez[2] · Nermeen Fawzy[3] · Robert Zimmermann[3] · Emily Eden[4] · Núria Casals[1,5] · Rosalía Rodríguez-Rodríguez[1,5]

✉ Núria Casals
ncasals@uic.es

✉ Rosalía Rodríguez-Rodríguez
rrodriguez@uic.es

[1] Department of Biomedical Sciences, Faculty of Medicine and Health Sciences, Universitat Internacional de Catalunya, 08195 Sant Cugat del Vallès, Spain

[2] Unit of Biophysics, Department of Biochemistry and Molecular Biology, Faculty of Medicine, Universitat Autònoma de Barcelona, 08193 Cerdanyola del Vallès, Spain

[3] Institute of Molecular Biosciences, Biochemistry, University of Graz, Graz, Austria

[4] University College London (UCL) Institute of Ophthalmology, London, UK

[5] Centro de Investigación Biomédica en Red de Fisiopatología de La Obesidad y La Nutrición (CIBEROBN), Instituto de Salud Carlos III, 28029 Madrid, Spain